

https://dspace.org/

The sintering and optimization of stabilised Zirconia.

Hoosain, Shaik Ebrahim.

2011-10-10
http://hdl.handle.net/10539/10517

Downloaded from a DSpace repository. https://dspace.org/

The Sintering and Optimization of Stabilised Zirconia

Shaik Ebrahim Hoosain

A dissertation submitted to the faculty of Engineering and the Built Environment, University of Witwatersrand, Johannesburg, in the fulfillment of the requirements for the degree of Master of Science.

Johannesburg, 2010

Declaration

I declare that this dissertation is my own unaided work, except where due acknowledgement for the assistance has been made. It is being submitted for the degree of Master of Science in Engineering at the University of Witwatersrand, Johannesburg. It has not been submitted before for any degree or examination at any other University.

_____

S.E. Hoosain

_____

Date

Abstract

Nano-sized 3 mol% yttria stabilised zirconia powders were synthesized from a co-precipitation technique and compared to powders obtained from Geratech Zirconium Beneficiation Ltd, a zirconium chemical plant company based in Johannesburg. The aim of this research was to investigate the possibility whether these powders could compete commercially with established international companies producing the same powder. The co-precipitated powder was then subjected to various calcination treatments. Both these powders were then characterized using XRD (including Rietveld refinement), SEM, and DTA/TGA.

These powders were then milled extensively and then uniaxially compressed into cylindrical pellets at 250 MPa. These resulting pellets were then subjected to sintering in air at various temperatures for two hours. The properties of the ceramic produced from these powders were assessed and compared to the commercial Wieland Zeno disc. The microstructural features and the phase composition were examined using SEM and Rietveld Refinement. The mechanical properties such as hardness and toughness were determined using Vickers indentations. Fracture strength values were obtained using standard three point bend tests. These mechanical properties were then compared to values obtained for bio-grade zirconia ceramics. Values obtained generally consistent with most of the previously published work and the theories behind the remarkable properties in zirconia-based ceramics. Sintering conditions played a major role in the properties obtained for the ceramic as these conditions all had an effect on grain size, phase composition, and relative density and porosity. All these factors were found to have an effect on the final properties of the ceramic.

Acknowledgements

Firstly, I would like to thank God, for guiding me through to where I am today and all the challenges I have faced. Also I would like to thank the following people:

My supervisors, Prof. I. Sigalas and Dr M. Herrmann, for their unwavering and patient support throughout this work, their attention to my academic and personal needs.

My friends and colleagues in the School of Chemical and Metallurgical Engineering.

My loved ones for their patience and their support. Thank you for being there when I needed you.

Geratech Zirconium Beneficiation Ltd and the Centre of Excellence for financial and technical support.

Table of Contents

Declaration……ii
Abstract……iii
Acknowledgements……...v
Table of Contents……..vi
List of Figures……...ix
List of Tables……xiii
1. Introduction…….... 1
1.1. Aims and Objectives……1
1.2. Structure of the dissertation…….2

2. Literature Review……...3
2.1. Structure and phase transformations of zirconia……4
2.1.1. Temperature dependent phases of zirconia……..5
2.2. The Zirconia-Yttria phase diagram……8
2.3. The tetragonal to monoclinic phase transformation……...11
2.3.1. Mechanisms, thermodynamics and kinetics of the transformation……11
2.3.2. Overview of Zirconia Ceramics……..16
2.3.2.1. Partially Stabilised Zirconia (PSZ)……..16
2.3.2.2. Cubic Stabilised Zirconia (CSZ) ……17
2.3.2.3. Tetragonal Zirconia Polycrystals (TZP)……..17
2.4. Grain size effects in Tetragonal Zirconia Polycrystals……..19
2.4.1 Critical Grain Size and Mechanical Properties……....19
2.4.2 Grain growth kinetics……. ……22
2.4.3 Grain growth mechanisms……....24
2.4.4. Grain growth mobility and activation energy……..25
2.5. Zirconia as a biomaterial……26

3. Experimental Procedure……29

3.1. Ceramic Preparation……29
3.1.1. Powder Preparation Method…….... .29
3.1.2. Calcination…… 30
3.1.3. Milling……...30
3.1.4. Particle Size Analysis……31
3.1.5. Binder Addition…… 31
3.1.6. Compaction……....31
3.1.7. Binder Burnout……..... 31
3.1.8. Sintering……32
3.2. Ceramic Characterization……....33
3.2.1. Density Measurements……..33
3.2.2. Thermal Etching……33
3.2.3. Vickers Hardness…….. 34
3.2.4. Indentation Fracture Toughness……....34
3.2.5. Scanning Electron Microscopy and grain Size Determination……..35
3.2.6. X-ray Diffraction……..36
3.2.7. Thermal Analysis……. 36
3.2.8. Three-point bend test…… 36

4. Results……....38
4.1. The Geratech powder……..38
4.1.1. X-ray diffraction data for the Geratech powder…….. 38
4.1.2. SEM of the powders supplied by Geratech……..40
4.1.3. Particle size analysis of the 3 mol% Yttria stabilised Zirconia powder supplied by Geratech Ltd…… 42
4.1.5. Compaction of the yttria stabilised zirconia powder supplied by Geratech…....44
4.2. Characterization of the sintered ceramic……....45
4.2.1. Densities and grain sizes of the ceramic after sintering…….. 45
4.2.2. SEM Micrographs of the ceramic sintered at various temperatures……47
4.2.3. XRD patterns of the ceramic sintered at various temperatures……48

4.2.4. Mechanical properties of the sintered ceramic from the
3Y-zirconia powder supplied by Geratech……..49
4.3. The co-precipitated powder…….. 50
4.3.1. DTA/TGA results of the prepared powder…… 51
4.3.2. Calcination of the co-precipitated powders……... 52
4.3.3. SEM of the co-precipitated 3mol% yttria stabilised ZrO_2 powder……... 54
4.3.4. Particle size distribution of the co-precipitated powder…… 55
4.4. Characterization of the sintered ceramic……....57
4.4.1. Density and grain size of the ceramic after sintering……..57
4.4.2. SEM Micrographs of the ceramic sintered at various temperatures…….. 58
4.4.3. XRD pattern of the sintered ceramic from the co-precipitated powder……. 59
4.4.4. Mechanical properties of the sintered ceramic from the co-precipitated
3Y-zirconia powder…… .60
4.5. Transverse Rupture Strength Results……61
4.6. The reference Zirconia biomaterial obtained from Wieland Zenotec……63

5. Discussion…… 66
5.1. Properties of the co-precipitated powder…… .66
5.1.1. Calcination study of the prepared powder…… .66
5.1.2. Compaction of the prepared powder…… .68
5.2. Properties of the co precipitated powder and the powder supplied by
Geratech……68
5.3. Properties of the sintered ceramic……..70
5.3.1. Comparison of the sinterability of the Geratech, the synthesized powders,
and the Wieland commercial compact……71
5.3.2. Hardness……... .72
5.3.3. Fracture toughness……. 73
5.4.4. Fracture Strength…….....75

6. Conclusions and Recommendations……76
6.1. Conclusion……76

6.2. Recommendations……....77

7. References……79

8. Appendices…… ..84

List of Figures

Figure 2.1: The unit cell of cubic zirconia. The green circles denote the Zr atoms and the purple circles the O atoms. Darker shades of green are used to portray Zr atoms toward the rear of the unit cell……..5

Figure 2.2: The unit cell of tetragonal zirconia. Small dark circles denote the Zr atoms and the large clear circles denote the O atoms. The arrows show the shift of O pairs[8]……6

Figure 2.3: The unit cell of monoclinic zirconia. The small dark circles denote Zr and the large clear circles denote the O atoms[8]……..7

Figure 2.4: low yttria region of the $YO_{1.5}$-ZrO_2 phase diagram[19]……...9

Figure 2.5: Phase diagrams for the $YO_{1.5}$-ZrO_2 (ZrO_2 portion), summarized by Yoshimura (1988)[22]……..10

Figure 2.6: Schematic views of the transformation zone and toughness increment, ΔK_c, development with crack extension……...15

Figure 2.7: Microstructure of yttria stabilised tetragonal zirconia[26]……..19

Figure 2.9: the critical grain size for spontaneous tetragonal to monoclinic transformation as a function of yttria content in zirconia[35]…….21

Figure 2.10: Grain sizes of differently doped zirconia as a function of soaking time at 1400°C (n = 3)[39]……...23

Figure 2.11: Variation in kinetic grain growth versus the inverse of temperature for cubic (8Y), tetragonal (3Y) and monoclinic (0Y) zirconia[41]…26

Figure 2.12: Microstructure of Bio-medical grade zirconia for dental applications[11]……...28

Figure3.1: Schematic of the preparation process for the zirconia ceramic…….32

Figure 3.2: Schematic of the Vickers hardness indentation showing the radial cracks produced by the diamond indentor……....35

Figure 4.1: XRD data for the monoclinic zirconia powder supplied by Geratech……..38

Figure 4.2: XRD pattern of the 3 mol% yttria stabilised powder supplied by Geratech……..39

Figure 4.3: SEM micrograph of the monoclinic powder supplied by Geratech……..41

Figure 4.4: micrograph of 3Y-zirconia supplied by Geratech……41

Figure 4.5: Particle size distribution of the initial powder supplied by Geratech Ltd……...42

Figure 4.6: particle size distribution of the yttria stabilised zirconia supplied by Geratech after 10 hours of milling…… 43

Figure 4.7: Compaction curve of the yttria stabilised powder supplied by Geratech……..... 44

Figure 4.8: SEM micrographs of the ceramic sintered at: a) 1450°C;
b) 1350°C; c) 1250°C; d) 1150°C, for two hours……47

Figure 4.9: XRD patterns of the ceramic sintered at temperatures a) 1250°C;
b) 1150°C. m = monoclinic phase……...49

Figure 4.10: DTA/TGA trace of the uncalcined 3Y-zirconia prepared
via the co-precipitation route……..52

Figure 4.11: XRD pattern of powder calcined at various temperatures;
A = 600°C, B = 700°C, C = 800°C, D = 900°C, E = 1000°C
* = monoclinic phase, all other peaks are tetragonal……..53

Figure 4.12: Electron micrograph of the prepared 3 mol %
yttria – stabilised zirconia calcined at 900°C for one hour…….55

Figure 4.13: particle size distribution of the co-precipitated powder
calcined at 900°C prior to milling……...55

Figure 4.14: Particle size distribution of the co-precipitated powder after
8 hours of milling……56

Figure 4.15: SEM micrographs of the ceramic sintered at: a) 1450°C;
b) 1350°C, for two hours……58

Figure 4.16: XRD patterns of the ceramic sintered at temperature 1450°C
for two hours…….. 59

Figure 4.17: XRD patterns of the fracture surfaces sintered at: a) 1450°C and b) 1350°C. All peaks are tetragonal unless otherwise shown *monoclinic phase……62

Figure 4.18: XRD pattern of the Wieland compact sintered at 1450°C for two hours……64

Figure 4.19: SEM micrograph of the Wieland ceramic sintered at 1450°C for two hours……64

Figure 5.1: The effect of calcination temperature on crystallite size of the powder…… 67

Figure 5.2: % tetragonal phase as a function of calcination temperature for the co-precipitated powder……. 69

Figure 5.3: the % theoretical density as a function of sintering temperature….. 71

Figure 5.4: Dependence of Vickers hardness on the sintering temperature of the Geratech powders and the co-precipitated powder……... 72

Figure 5.5: Fracture toughness as a function of sintering temperature for the ceramic using the co-precipitated and the Geratech powder……... 73

List of Tables

Table 1: Summary of the different phases of zirconia…….. 8
Table 2: Mechanical properties of the various types of zirconia ceramics……..16
Table 3.1: Chemicals used in the co-precipitation method……..30
Table 4.1: XRD data for the Geratech powders…….. 39
Table 4.2: Effect of time on particle size of the 3 mol% yttria stabilised zirconia powder supplied by Geratech…….43
Table 4.3: Densities of the sintered ceramic as a function of temperature sintered for two hours……...46
Table 4.4: Summary of the mechanical properties of the sintered ceramic at various temperatures……...50
Table 4.5: XRD data of the 3Y-ZrO_2 powder obtained after various thermal treatments for one hour……. ...54
Table 4.6: Effect of milling time on particle size……..57
Table 4.7: Densities of the sintered ceramic as a function of temperature sintered for two hours…….. 58
Table 4.8: Summary of the mechanical properties of the sintered ceramic at various temperatures……... 60
Table 4.9: TRS results of the ceramic made from the 3Y-zirconia powder from Geratech……... 61
Table 4.10: Densities of the Wieland sintered ceramic as a function of temperature sintered for two hours……..63
Table 4.11: Summary of the mechanical properties of the Wieland Zirconia disc according to manufacturer's specifications……....65

Chapter 1: Introduction

Advanced ceramics is a fast growing market and there is currently a wide range of developments that have the potential to show further growth. In particular, developments in telecommunications, catalyst systems, solid oxide fuel cells and bio-ceramics are expected to boost demand for specific high purity oxides significantly.

The zirconium downstream industry has an estimated global demand for more than 100 000mt of chemicals and more than 10 000mt of chemically precipitated Zr oxides per annum. It is a larger than $500 million industry that continuously grows as technology advances across a diversified spectrum of industries. Significantly, South Africa produces approximately half of the world's zircon ($ZrSiO_4$)[56].

The remarkable mechanical properties of zirconia, already exploited in several medical and engineering applications, are mainly due to the tetragonal to monoclinic (t-m) phase transformation. The t-m transformation, which can be induced by external stresses, such as grinding, cooling and impact, results in a 4% increase of volume[7,11] that causes compressive stresses. These stresses may develop on a ground surface or in the vicinity of a crack tip. It is this clamping constraint about the crack tip that must be overcome by the crack in order to propagate, explaining the increased fracture toughness of zirconia compared to other ceramics. Yttrium stabilized zirconia is considered to be one of the most promising structural materials for mechanical applications because of their excellent bending strength and fracture toughness. In the ZrO_2-Y_2O_3 system, the ideal microstructure for high strength and high toughness is the single tetragonal phase with fine and uniform grains (0.2-1µm) containing approximately 3 mol% Y_2O_3.

1.1. Aims and Objectives

This project is a joint effort by a company called Geratech Zirconium Beneficiation Ltd and the University of the Witwatersrand. Geratech Zirconium Beneficiation Ltd is an established company that beneficiates the mineral zircon to produce a range of chemicals that have applications in a diversity of industries. The mineral zircon is mined mainly in

Australia and South Africa. Geratech Zirconium Beneficiation uses this locally mined mineral as feed to produce its finished products and is the only zircon chemical beneficiation plant in Africa.

The aim of this project is to use the available resources to produce a zirconia ceramic to be used for dental applications and to match the properties of the corresponding commercially available ceramics. In the past, the raw material would be exported overseas for further processing (since S.A. did not have the necessary skills or technology) and the end product would be supplied from Europe at a massive profit (due to the low cost of raw material compared to the end product). Since these zirconia ceramics are mainly supplied from European companies, Geratech aims to infiltrate this lucrative market by using locally supplied raw material and to develop the technology and skills to produce the zirconia ceramic at a competitive price.

1.2. Structure of the dissertation

In the introduction, the background to the project and the aim of the project are discussed. A literature review then follows which includes a brief overview of zirconia, the zirconia-yttria phase diagram, the tetragonal to monoclinic transformation including the thermodynamics, the strengthening mechanisms (strength, toughness, and hardness), and bio-medical grade zirconia. The detailed experimental procedure is discussed in chapter 3 including characterization techniques. Chapter 4 contains the results of the experimental procedures followed by a discussion of these results in chapter 5. Conclusions and recommendations are then made in chapter 6.

Chapter 2: Literature Review

Zirconia is one of such ceramic materials described in section 1 that exhibit high hardness, corrosion and erosion resistance, as well as having additional toughness due to a stress induced phase transformation[3,4,5,6]. Zirconia based ceramics are also well-known for their excellent electronic, thermal and optical properties. This kind of ceramic is fully employed in various applications such as oxygen sensors, fuel cells and dental ware because of its good oxygen ion conductivity and excellent mechanical properties[3,4,5].

The great potential offered by the mechanical and electrical properties of zirconia and zirconia-containing ceramics has led to much work on fabrication procedures capable of providing homogeneous and reproducible materials with closely defined microstructures.

Zirconia exhibits polymorphism: it exists in three crystalline forms, namely monoclinic (m), tetragonal (t) and cubic (c)[6]. At room temperature zirconia is stable in the monoclinic structure and changes to the tetragonal structure at about 1100°C, transforming to the cubic structure at about 2300°C, upon heating. The phase transformations are reversible upon cooling with the tetragonal to monoclinic transformation being the most studied. The transformation of pure zirconia from the m-phase to the t-phase is accompanied by a volume increase of about 4-5% causing cracking and structural failure[6,7]. This volume increase of pure zirconia makes it unsuitable for any application[8]. However, to stabilise the high temperature t-phase at room temperature, appropriate amounts of divalent, trivalent or lanthanide oxides such as MgO, CaO, CeO_2 and Y_2O_3 can be alloyed to pure zirconia[5,6,9]. This was found to give zirconia based ceramics high strength and exceptionally high fracture toughness for a ceramic. The addition of 3 mol% yttria was found to be sufficient to stabilise the t-phase at room temperature. Yttria was found to reduce the t-m transformation temperature from 1100°C to approximately 550°C[10,11]. At this temperature the t-phase can be retained to room temperature as there is not sufficient amount of energy for the t-m transformation to occur.

In the ZrO_2-Y_2O_3 system, the ideal microstructure is the single tetragonal phase as it leads to an increase in strength, hardness, and fracture toughness of the sintered zirconia materials[11,12]. The high toughness is due to a phase transformation induced by the stress relief due to a crack propagating in the metastable t-phase. The increase in volume accompanying transformation causes compressive stresses and these stresses may develop on a ground surface or in the vicinity of a crack tip. It is this clamping constraint about the crack tip that must be overcome by the crack in order to propagate, explaining the increased fracture toughness of zirconia compared to other ceramics[7].

The mechanical properties of zirconia based ceramics depend on the microstructure and composition and can be controlled to obtain the required properties. Zirconia has a high melting point, a high ductile to brittle transition temperature and is a good thermal insulator. At room temperature it is an electrical insulator but when alloyed with trivalent oxides it becomes an ionic conductor at high temperatures. Zirconia is colorless, transparent and has a high refractive index. These combinations of properties and the ability to manipulate its structure, makes zirconia useful in various applications including refractories, medical implants, catalysts, ionic conductors in solid fuel cells and in toughening components in nano-composites[8].

2.1. Structure and phase transformations of zirconia

Zirconia has been found to change phase under certain temperatures and pressures. At normal atmospheric pressure the oxide is monoclinic at room temperature. It then transforms to the tetragonal and cubic phases with an increase in temperature. The oxide also transforms to an orthorhombic I (OI) phase and then to an orthorhombic II (OII) phase with increasing pressure. For the scope of this project only the phase transformations occurring at atmospheric pressure are discussed.

2.1.1. Temperature dependent phases of zirconia

a) The cubic phase (c)

The cubic phase (c) of zirconia is stable at approximately 2370°C and above up to its melting point[3,4,7,14]. The structure is based on the fluorite (Ca_2F) structure in which each Zr atom is coordinated by eight octahedrally-placed equidistant oxygen atoms, each at a distance of 22.19nm. Each oxygen ion is tetrahedrally coordinated by four zirconium atoms. Figure 2.1 below shows the crystal structure of cubic zirconia:

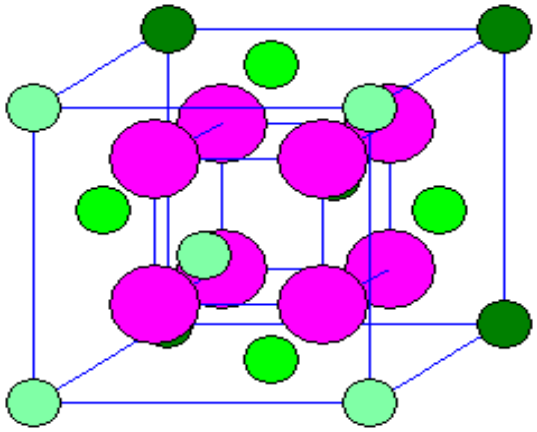


Figure 2.1: The unit cell of cubic zirconia. The green circles denote the Zr atoms and the purple circles the O atoms. Darker shades of green are used to portray Zr atoms toward the rear of the unit cell[8].

This can be visualised by the cations occupying the face centred cubic positions in the cubic lattice, with eight interstitial O atoms and a large vacancy in the middle as shown in Figure 2.1. The space group of this structure is *Fm3m* and the values suggested for the lattice parameter a, is approximately 0.512nm for zirconia[15].

b) The tetragonal phase (t)

The tetragonal phase is thermodynamically stable from approximately 1100°C to 2370°C in zirconia[3,4,7]. This crystal structure resembles the cubic structure as shown in figure 2.1 with two important differences:

- There is a distortion in the crystal lattice corresponding to a slight elongation along the c-axis

- There is a displacement of alternate O atom columns along the c-axis

Each Zr atom maintains its eight-fold coordination of O atoms, four at a distance of 2.455Å and the other four at a distance of 2.065Å. The space group of this structure is $P4_2/nmc$, with lattice parameters a = 0.5094nm and c = 0.5177nm. Figure 2.2 shows the crystal structure of tetragonal zirconia[16]:

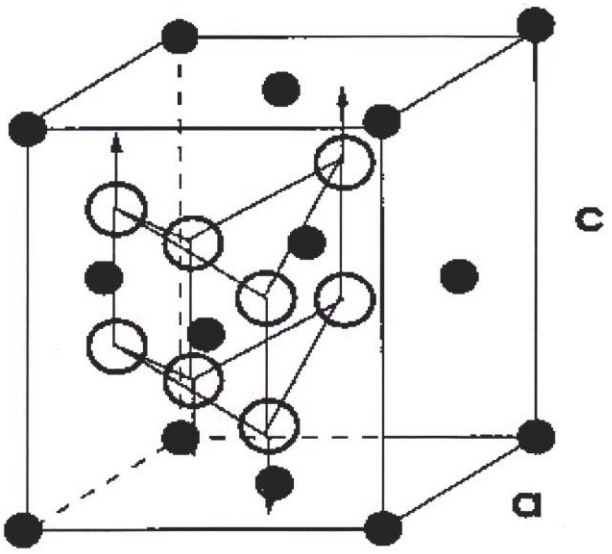


Figure 2.2: The unit cell of tetragonal zirconia. Small dark circles denote the Zr atoms and the large clear circles denote the O atoms. The arrows show the shift of O pairs[8].

For ZrO_2, the x-ray diffraction pattern for the tetragonal phase is almost identical to that of the cubic phase except for the splitting of a number of peaks to form doublets caused by the elongation of the c-axis. If the peaks are broad due to small crystallite size, it can be complex to distinguish between the t and c phases unless high angled peaks are examined or vibrational spectroscopy is used[17].

c) The monoclinic phase (m)

The monoclinic phase is thermodynamically stable in zirconia at temperatures below 1100°C[3,4,6,7]. The unit cell can be described as a distorted cubic cell although the structure is considerably more complex than the cubic and tetragonal phases. Figure 2.3 shows the structure of monoclinic zirconia:

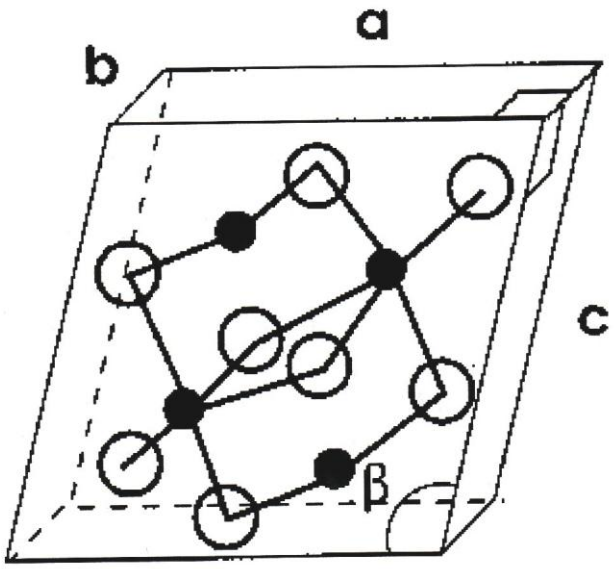


Figure 2.3: The unit cell of monoclinic zirconia. The small dark circles denote Zr and the large clear circles denote the O atoms[8].

Each Zr atom in the monoclinic structure is coordinated by seven O atoms with varying bond lengths and a range of O-Zr-O bond angles. The O atoms are arranged in two parallel (100) planes, separated by layers of Zr atoms. The space group of this structure is $P2_1/c$[14], with lattice parameters a = 0.51454nm, b = 0.52075nm, c = 0.53107nm, and β = 99.18° [18].

Table 1 summarizes the three phases as discussed:

Table 1: Summary of the different phases of zirconia

Phase	Space Group	Lattice Parameters (nm)			Density (g/cm^3)
		a	b	c	
Monoclinic	**$P2_1/c$**	**0.51454**	**0.52075**	**0.53107**	**5.83**
Tetragonal	**$P4_2/nmc$**	**0.5094**	**0.512**	**0.5177**	**6.08**
Cubic	**Fm3m**	**0.512**	**0.512**	**0.512**	**5.65**

2.2. The Zirconia-Yttria Phase Diagram

In order to understand the behaviour of zirconia ceramic materials, it is essential to refer to the phase equilibria in those zirconia systems known to produce stabilised zirconia ceramics. Additions of relatively small amounts of certain oxides to zirconia will alter the relative stability of the phases. The transformation temperatures fall and the tetragonal or cubic phase may become stable or metastable at room temperature. The oxides used to achieve this effect are usually divalent or trivalent metals such as magneia (MgO), calcia (CaO), yttria (Y_2O_3) etc. For the scope of this project the zirconia-yttria system is discussed.

Y-TZP (Yttria stabilised Tetragonal Zirconia Polycrystals) represent the most important class of zirconia ceramics. In order to produce useful ceramics from zirconia, it is essential to form a solid solution between the dopant and zirconia. A major factor affecting the potential for solid solution formation in zirconia binary systems appears to be the size of the dopant ion, which gives an indication as to whether the ion can be accommodated in the zirconia structure and hence form a solid solution.

Due to the importance of yttria stabilised zirconia as an engineering ceramic material, extensive work has been done on the establishment of the $YO_{1.5}$-ZrO_2 phase diagram[19,20], especially the zirconia rich portion thereof, but the different phase diagrams contain inconsistencies in the locations of the phase boundaries.

The work of Scott (1975)[19] is considered the most accurate at temperatures above 1450°C (figure 2.4) and his results have been confirmed by Jayaratna (1984)[21] at 1600°C. A feature observed in the $YO_{1.5}$-ZrO_2 phase diagram is the decrease in the tetragonal to

monoclinic phase transformation temperature with increasing dopant or yttria content. This phenomenon is significant in ceramic materials since it affects the useful temperature ranges of application of the various compositions.

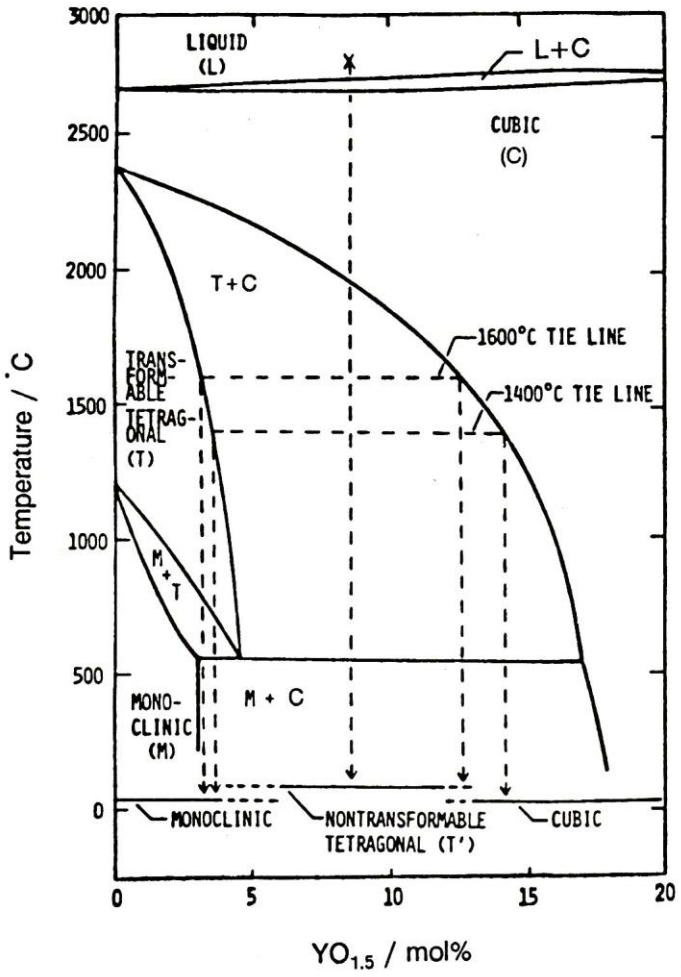


Figure 2.4: Low yttria region of the $YO_{1.5}$-ZrO_2 phase diagram[19].

Above the monoclinic phase field there is a small monoclinic and tetragonal (M + T) phase field (0-4 mol% yttria). At higher temperatures the system has a transformable tetragonal phase field (< 5 mol% yttria). High yttria content tetragonal compositions are non-transformable (termed T' phase). This non-transformable T' phase itself arises from a transformation of cubic phase on cooling. This material is derived from the two phase tetragonal + cubic (T+C) region. Further increases in the yttria content results in a fully stabilised cubic region. The slope of the line dividing the T and T + C region is of great

significance. On sintering a fixed composition material at increasing temperatures from 1300°C upwards, the proportion of the cubic phase will increase with increasing temperatures by the lever rule[19].

Figure 2.5 shows Yoshimura's (1988)[22] summary of the zirconia-rich portion of the phase diagram indicating the large number of variations in the phase diagram studies, especially at the tetragonal/tetragonal + cubic phase boundary, which is within the sintering temperature range of zirconia ceramic materials. The variations found in the phase boundaries reported by different workers probably represent the same transition but different kinetics probably due to the extensive times required to reach equilibrium. This behaviour is observed in all binary zirconia systems and makes the accurate prediction of the phases of the sintered ceramic difficult[21,22].

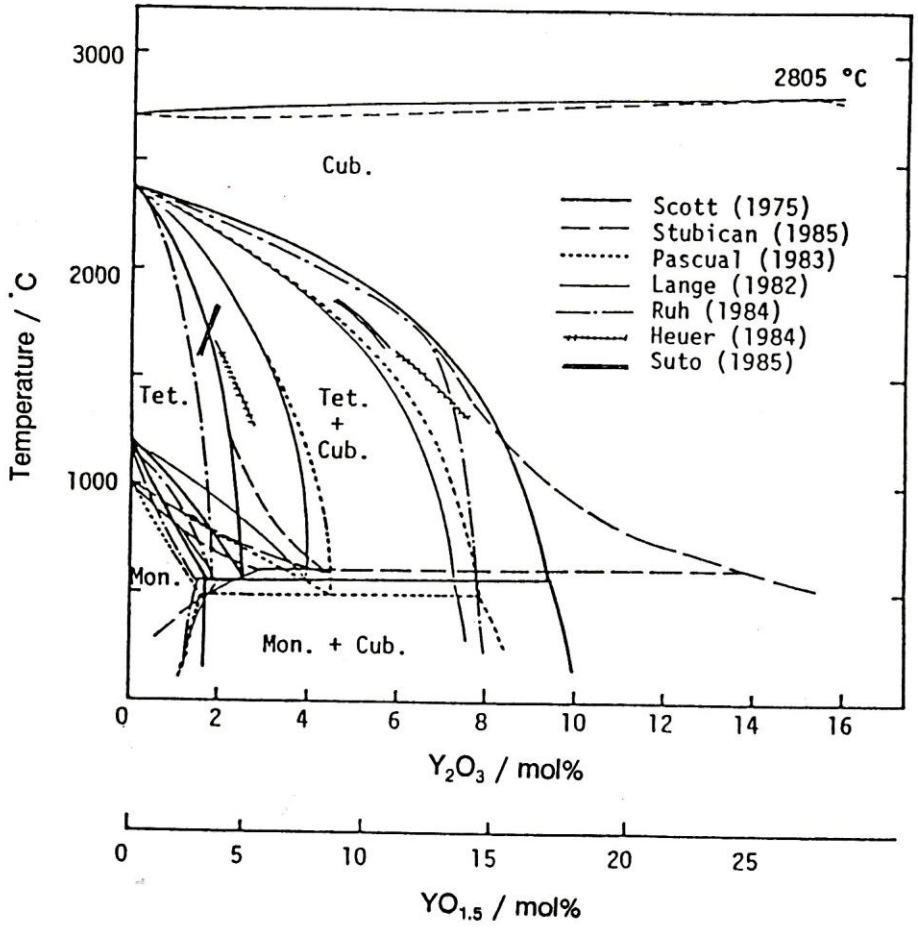


Figure 2.5: Phase diagrams for the $YO_{1.5}$-ZrO_2 (ZrO_2 portion) , summarized by Yoshimura (1988)[22].

2.3 The Tetragonal to Monoclinic Transformation

Patil and Subbaroa (1970)[23] undertook high temperature X-ray diffraction studies on zirconia. They found that the tetragonal to monoclinic phase transformation in zirconia is martensitic; that is, it takes place via a diffusionless shear-like mechanism, where the atoms retain their neighbours in both phases[24]. Based on their research the high temperature tetragonal phase cannot be quenched to room temperature in undoped oxides. This transformation involves a change in coordination of the Zr ion from eight to seven with an associated, unusual volume increase of 3-5%. This has practical importance for zirconia based ceramics in two respects:

- The expansion causes considerable cracking in dense zirconia when cooled through the transition temperature. This explains why pure zirconia monoliths are not prepared.

- This transformation leads to 'transformation toughening' of partially stabilised zirconia ceramics.

This volume expansion is sufficient to exceed elastic and fracture limits in large grains and specimens and can only be accommodated by sample cracking. The t-m transformation on cooling sintered ZrO_2 prevents the exceptional refractory properties of pure zirconia from being utilized in structural ceramics.
ZrO_2 is strongly anisotropic in thermal expansion, with the b-axis exhibiting negligible expansion while substantial expansions are observed for the a- and c-axes[23].

2.3.1 Mechanisms, thermodynamics and kinetics of the transformation

There is general agreement that the transformation involves both nucleation and subsequent growth processes and the transformation is nucleation-controlled. Two conflicting theories have been proposed to interpret how the nucleation of the martensitic transformation is induced:

a) The 'Non-classical' Model[24]

This model involves a continuous sequence of states along the reaction path i.e. locally "there is a continuous distortion of the parent phase into the martensitic product in small, finite regions until a critical-sized nucleus of the martensitic product is reached". Therefore the nucleation is homogeneous. On the basis of in-situ microstructural observation (TEM) and thermodynamic data, it was suggested that the nucleation was assisted by stress. This stress arises from thermal expansion mismatch, microstructural defects and morphology effects.

b) The Classical Model[25]

This model proposes that the nucleation is a "heterogeneous process with the formation of the martensitic nucleus being a sudden occurrence. It is thermodynamically assisted by stresses related to microstructural defects, such as micro-cracks, concentration gradients, and lattice defects". Chen and Chaio (1985)[25] established a clear relationship between particle size and the possibility of nucleating the martensitic product.

Two main phenomena resulting from the transformation include:

(1) increased resistance for growth of both short (≤100μm) and long (≥0.3mm) cracks,
(2) Toughness continuing to increase with crack length (termed R-curve behavior) until generally reaching a toughness plateau[26].

These lattice transformations are martensitic, characterized by being:

- Diffusionless
- Occurring athermally, implying the need for a temperature change over a range rather than at a specific temperature
- Involving a shape deformation.

This transformation range is bounded by the martensitic start (M_s) and martensitic finish temperatures[26].

These transforming ceramics step away from the simple Griffith dependence on flaw size[26] and many have strengths that depend on the stress needed to trigger transformation imposing flaw-size sensitivity. Driving forces and the role of temperature particularly for the t-m transformation can be thermodynamically considered; the total unit volume free energy change ΔF for the transformation, including an applied stress is:

$$\Delta F = \Delta F_{CH} + \Delta U_e + \Delta U_s - \Delta U_l \quad \text{(eq 1)}$$

Where ΔF_{CH} is the chemical free energy change,
ΔU_e is the strain energy change,
ΔU_s is the surface energy change, and
ΔU_l is the interaction term due to stress application

The surface free energy change is considered negligible and the chemical free energy term can be stated as a function of transformation entropy change $\Delta S^{t\text{-}m}$ and temperature[11,12,26]:

$$\Delta F_{CH} = \Delta S^{t\text{-}m} (T_0 - T) \quad \text{(eq 2)}$$

Where T is the test temperature and T_0 is the transformation temperature for an unconstrained t-phase particle. Tetragonal particles embedded within a matrix will be stabilized by both matrix constraint as well as the strain energy term ΔUe. Constrained particles, that are metastable, will transform at a temperature $M_s < T_0$ (with M_s being the martensitic start temperature). Dopants such as Y_2O_3 act to decrease both the M_s and T_0 temperatures. This decrease in M_s below T_0 creates an additional free energy change term capturing matrix and dopant stabilization, equal to $\Delta S^{t\text{-}m} (T_0 - M_s)$. Therefore, without an applied stress the free energy change accompanying the transformation can be expressed as follows:

$$\Delta F = \Delta S^{t\text{-}m} [(T_0 - T) - (T_0 - M_s)] = \Delta S^{t\text{-}m} (M_s - T), \quad \text{(eq 3)}$$

noting that $\Delta F = 0$ at $T = M_s$, initiating transformation.

At service temperatures above M_s, an applied stress U_l can reduce ΔF to zero and trigger the t-m transformation:

$$\Delta F = \Delta S^{t\text{-}m}(M_s - T) - U_l \qquad \text{(eq 4)}$$

By defining the interaction term U_l in terms of an applied stress σ_a and the transformation dilatational strain ε^T:

$$\Delta U_l = \sigma_a \varepsilon^T \qquad \text{(eq 5)}$$

Now the critical applied stress for transformation $\sigma_c{}^T$ becomes

$$\sigma_a = \sigma_c{}^T = \Delta S^{t\text{-}m}(M_s - T)/\varepsilon^T \qquad \text{(eq 6)}$$

Two practical implications arise from this analysis:

- The stress required for transformation increases with temperature above M_s and
- at a given temperature (above M_s) this critical applied stress will increase as M_s is decreased.

The kinetics of transformation is governed by nucleation, with the probability of nucleation enhanced by local residual stresses as well as an applied stress. Transformation involves the development of a *transformation zone* associated with the crack tip. The size and features of the zone microstructure (grain size and micro-cracking) control toughening. The simplest, most common toughening mechanism concept involves crack-tip shielding (from the applied stress) by the compressive dilatational stress associated with transformation. It is now thought that a purely dilatant transformation within an included angle of 120° ahead of the crack tip leads to a decrease in toughness[11,26]. Other toughening factors relate to the microstructure of the transformed material that act both locally near the crack tip and in the crack wake. For example, the

crack tip is embedded in a micro-cracked material having an elastic modulus that differs from the bulk ceramic, creating an additional crack tip shielding term[26,27,28]. As cracks grow to a certain length, the toughness reaches a plateau determined by the crack-tip toughness mechanisms. Elements of this concept are presented schematically in figure 2.6:

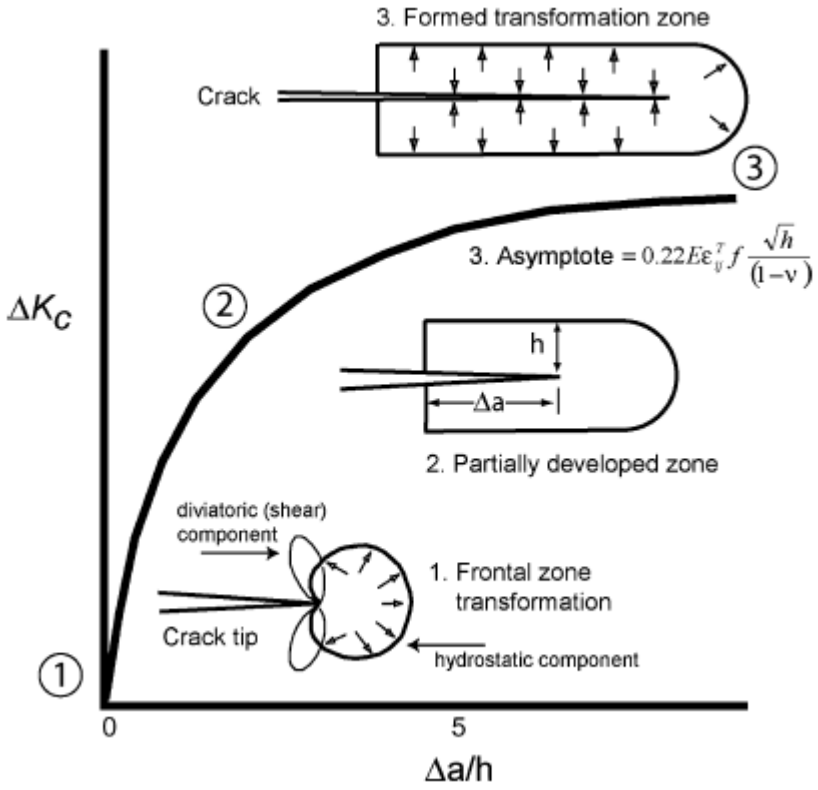


Figure 2.6: Schematic views of the transformation zone and toughness increment, ΔK_c, development with crack extension. Equation 3 in the figure represents the toughening increment where E is the local modulus of the transformed material, h is the width of the transformation zone, *f* the volume fraction of transformable phase, ε^T the dilatational strain, and v Poisson's ratio. (1) crack deflection and crack branching; (2) contact shielding by wedging and bridging involving broken-out grains or rough crack-wake surfaces and (3) stress-induced zone shielding involving transformation, microcracking and residual stress fields[26].

The size of the transformation zone was found to be a function of temperature and grain size, increasing as T drops to M_s and increasing as grain size increases. Zone size as a function of temperature (relative to M_s) has been visually demonstrated by Becher and

Swain (1992)[28] for Y-TZP and plays a critical role in the toughness increment achieved as a result of the microstructural changes occurring with transformation[12,26,28].

2.3.2. Overview of Zirconia Ceramics

Table 2 summarizes the properties of three types of zirconia ceramics. This is then followed by a description of the ceramics.

Table 2: Mechanical properties of the various types of zirconia ceramics

Type of zirconia ceramic	**PSZ[51]**	**CSZ[51]**	**TZP[29]**	**Biomedical grade zirconia[52]**
Density (g/cm^3)	5.5	5.65	6.04	> 6.0
Vicker's Hardness (H_v)	1100	1300	1300	1300
Flexural strength (MPa)	400-620	700	1200	1100
Elastic Modulus (GPa)	200	222	206	210
Toughness ($MPa.m^{1/2}$)	6	4	6-7	6-7

PSZ: Partially Stabilised Zirconia
CSZ: Cubic Stabilised Zirconia
TZP: Tetragonal Zirconia Polycrystals

2.3.2.1. Partially Stabilised Zirconia (PSZ)

The PSZ is an MgO partially stabilized zirconia often designated Mg-PSZ consisting of uniformly dispersed tetragonal precipitates in larger cubic phase crystals. Usually such PSZ consists of larger than 8 mol% (2.77 wt%) of MgO, 8 mol% (3.81 wt%) of CaO, or 3-4 mol% (5.4-7.1 wt%) of Y_2O_3. PSZ is a transformation-toughened material. The pure zirconia particles in PSZ can metastably retain the high-temperature tetragonal phase. The cubic matrix provides a compressive force that maintains the tetragonal phase. Stress energies from propagating cracks cause the transition from the metastable tetragonal to the stable monoclinic zirconia. The energy used by this transformation is sufficient to slow or stop propagation of the cracks[51].

2.3.2.2. Cubic Stabilised Zirconia (CSZ)

Generally, an addition of more than 16 mol% of CaO (7.9 wt%), 16 mol% MgO (5.86 wt%), or 8 mol% of Y_2O_3 (13.75 wt%) into zirconia is needed to form fully stabilized zirconia. Its structure becomes a cubic solid solution, which has no phase transformation from room temperature up to 2,500° C[51].

2.3.2.3. Tetragonal Zirconia Polycrystals (TZP)

Tetragonal zirconia polycrystals is a type of zirconia ceramic in which all the material is in the metastable tetragonal phase. These materials possess excellent mechanical properties at room temperature. Table 2 shows the reported mechanical properties of the TZP ceramic.

With the recognition that the transformation of the tetragonal phase to the monoclinic was responsible for the enhanced mechanical properties in zirconia ceramics, fully tetragonal phased zirconia ceramics were sought. The preparation of zirconia ceramic materials consisting of 100% tetragonal phase was first reported by Gupta *et al*. (1977)[29]. Ceramic powders were produced from water soluble yttria (e.g., YCl_3) and zirconia $ZrOCl_2$ precursors. When sintered, the resulting ceramics were found to be fine-grained, dense and fully tetragonal if sintered at temperatures below 1500°C. The proportion of cubic phase was found to increase at the expense of the tetragonal phase at sintering temperatures above 1500°C, due to the cubic phase becoming more stable at these higher temperatures. High strengths coincided with high tetragonal phase content and low strengths coincided with high monoclinic phase content. Subsequent investigation revealed that the highest strength and toughness was only found below a critical average grain size (<0.3μm). Many attributes are still shared with other polycrystalline materials, including the simplicity of processing, and the opportunity to explore chemistry-based powder fabrication and nano-scale microstructures. These materials consist primarily of equiaxed grains of tetragonal-zirconia sintered to approximately 98% of the theoretical density. Properties of these essentially homogeneous ceramics are primarily a function of

grain size, in that grain size controls the M_s temperature and the ease of transformation (and hence the toughness effect). The closer the test or service temperature is to the M_s temperature (but still above it avoiding spontaneous transformation) the less stable are the *t* grains and the higher the toughness increment. For a given dopant concentration the toughness increment decreases as grains become much smaller than the critical size, presumably due to "over-stabilization" of the grains, eliminating the t-m transformation upon introduction of a crack. This grain size effect is controlled by the dopant and dopant concentration[11,26]. The nature of the dopant essentially determines:

- The degree of tetragonality (the crystal lattice length ratio c/a, being > 1.0)
- The thermal expansion anisotropy (c verse a directions) of the unit cells.

In general higher tetragonality contributes to a less stable material characterized by an increase in M_s temperature. Based on tetragonality, at similar grain sizes and dopant concentrations yttrium appears to be a stronger stabiliser than cerium and magnesium. Anisotropic thermal expansion, for the *c* and *a* axes, can influence residual strains in *t* grains; higher residual stresses can lower the nucleation stress threshold for the *t-m* in the presence of crack-tip strain energy. It was reported in 2002 that the trend toward increased phase stability with decreasing particle-size of *t*-ZrO_2 could be overcome by adjusting the yttria dopant concentration[26]. Whereas 3mol% Y_2O_3 has been found to optimize toughness in micrometer and sub-micrometer *t*-ZrO_2, dopant concentrations and critical grain size for nano-scale material were identified as 1.0mol% for 90nm and 1.5mol% for 110 nm; both combinations reaching fracture toughness in the vicinity of $16MPam^{1/2}$ [26,30]. As with micro-scale zirconia, strong grain size effects (decreasing toughness with decreasing grain size) were exhibited in these nano-scale ceramics as well. Figure 2.7 depicts a micrograph of yttria-stabilised tetragonal zirconia:

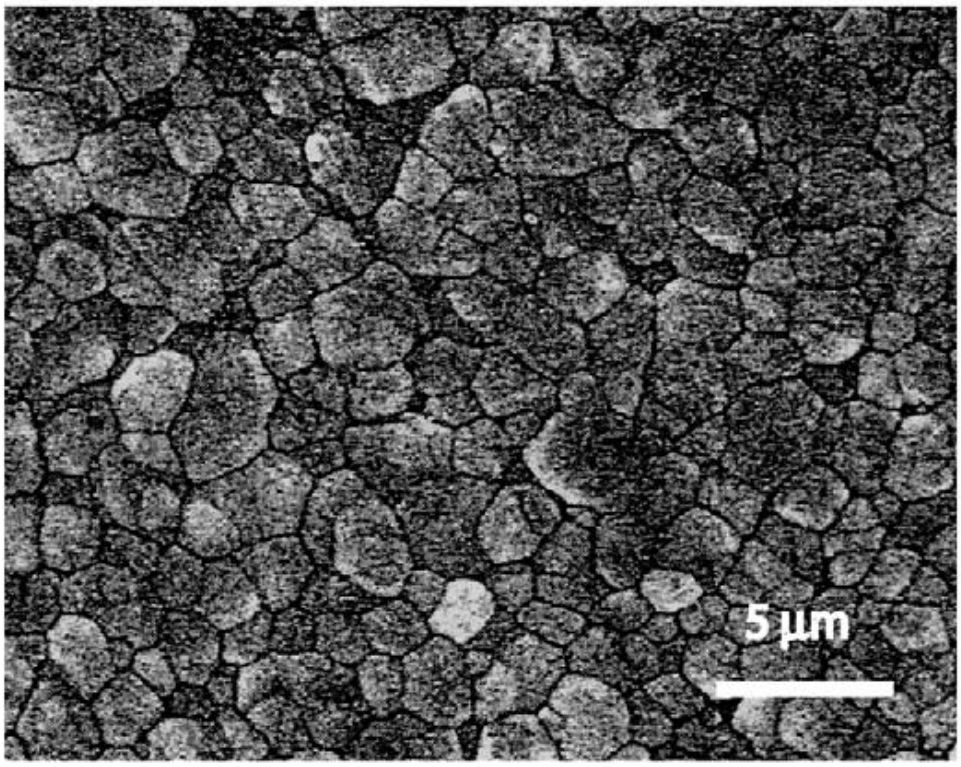


Figure 2.7: Microstructure of yttria stabilised tetragonal zirconia[26].

2.4. Grain size effects in Tetragonal Zirconia Polycrystals

2.4.1 Critical Grain Size and Mechanical Properties

The mechanical properties of Y-TZP strongly depend on its grain size. Above a critical grain size Y-TZP is less stable and more susceptible to the spontaneous t-m transformation whereas smaller grain sizes (< 1µm) are associated with a lower transformation rate. Consequently, the sintering conditions have a strong impact on both the stability and mechanical properties of the final product as they dictate the grain size. Higher sintering temperatures and longer sintering times lead to larger grain sizes[11]. Additionally, reduction in grain size of the powder changes the sintering behaviour of the ceramic material. The sintering temperature of nanocrystalline zirconia is 400-500°C lower than that of microcrystalline zirconia[30].

The sintering of ultrafine and nanocrystalline ceramics exhibits certain specific features. The high surface area of the particles provides a high driving force for sintering. Since

the diffusion distances are reduced, the rate of sintering increases. However, the nanocrystalline particles promote grain growth even at low temperatures. Wang *et al.*[32] studied the influence of grain size on three-point bending strength and Vickers fracture toughness. Initially, the fracture strength increased linearly for 3Y-TZP from 650 MPa at 0.9 μm grain size up to 1000 MPa for a critical grain size of 1.4 μm, after which it decreased to 750 MPa for a grain size of 1.8 μm. The grain size influence is related to the critical grain size for constraint phase transformation during mechanical loading. The decrease is caused by premature transformation, which causes microcracking and lowers the fracture strength. The change in fracture strength is mainly governed by the change in fracture toughness for the grain size regime of 0.9–1.8 μm. Basu *et al.* (2004)[33] investigated the indentation toughness of the zirconia ceramics as a function of mean grain size. The indentation toughness of the ceramic increases with increasing grain size until an upper critical grain size is exceeded; the subsequent decrease in toughness can be attributed to spontaneous transformation as the critical grain size has been exceeded.

Gupta *et al.* (1977)[30] reported that fine grain ZrO_2 (generally < 0.5μm) with small concentrations of stabilizing Y_2O_3 could contain up to 98% of the metastable *t* phase following sintering. High strengths coincided with high tetragonal phase content and low strengths coincided with high monoclinic phase content. Subsequent investigation revealed that the highest strengths and toughness were only found below a critical average grain size (<0.3μm). The results of Wang[32] and Gupta[30] confirm the existence of a critical grain size relating to the mechanical properties.

Nettleship *et al.* (1987)[34] attributed the effect of sintering temperature on strength as being due to the change in the grain size. The rapid increase in strength with decrease in the grain size in the range 0.34 to 0.3 μm cannot be explained by a conventional decrease in flaw size with grain size argument. It can be explained as an increasing contribution of the stress-induced phase transformation. Low strength samples with grain sizes above 0.34μm showed cracking on the external surface accompanying large amounts of t-m transformation. This supports the existence of a critical grain size for TZP and is consistent with the concept of the constrained transformation. Constrained transformation theory also indicates that such a transformation can be affected by stabiliser content.

Various authors have studied this effect on both physical and mechanical properties. Lange (1982)[35] compared grain size measurements with phase contents of as-sintered surfaces. Figure 2.9 shows how the stabiliser content was found to affect the critical grain size on an as-sintered surface. High tetragonal contents could not be achieved below 2% Y_2O_3 and the critical grain size rises sharply between 2% Y_2O_3 and 3% Y_2O_3. Unfortunately the sintered densities of Lange's specimens were in the range 80-90% of theoretical, and larger critical grain sizes might well have been achieved with a dense ceramic.

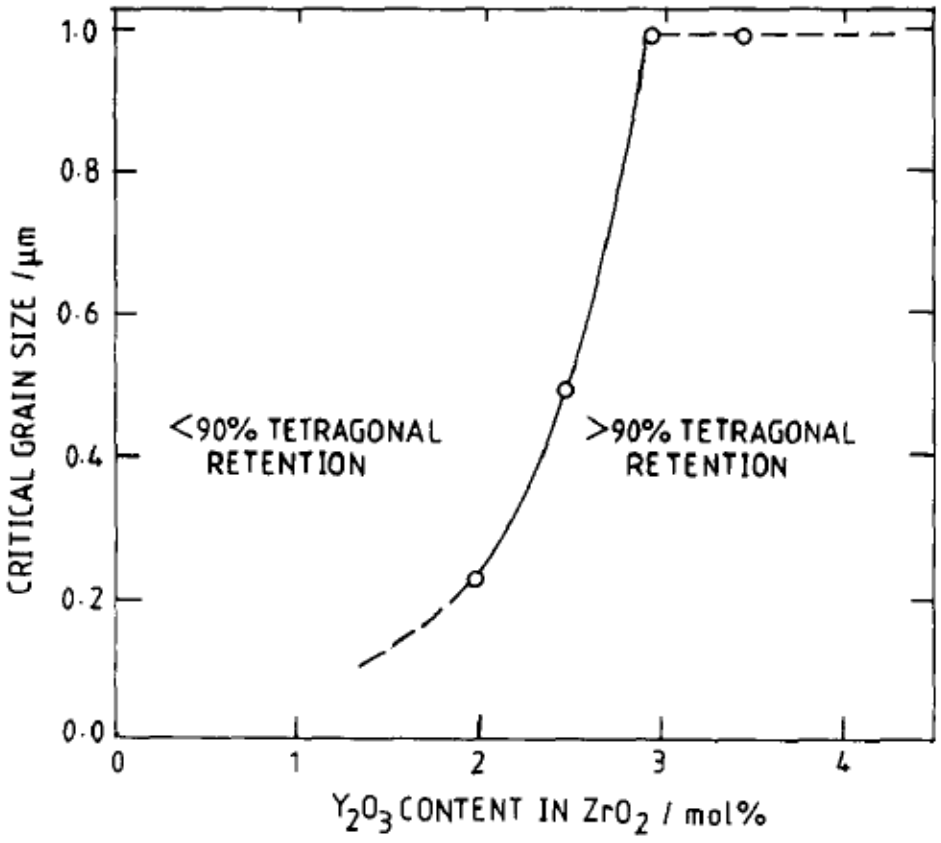


Figure 2.9: The critical grain size for spontaneous tetragonal to monoclinic transformation as a function of yttria content in zirconia[35].

Garvie *et. al.* (1975)[9] and Theunissen *et.al.* (1992)[36] derived an equation in which the critical grain size (d_c) for transformation is described as a function of the M_s temperature:

$1/d_c = (C1 + C2)*M_s$ (eq 7)

C1 and C2 are constants. The M_s temperature is a measure of the thermal stability. The thermal stability increases with decreasing M_s. If d (grain size) < d_c the tetragonal structure is retained at or above the M_s temperature. When measuring M_s temperatures it has to be ensured that only the grain size effect is measured. This implies similar densities for all samples.

2.4.2 Grain growth kinetics

Pressureless sintering and densification of nanocrystalline oxide powders are often accompanied by grain growth, the process by which the ceramic loses its nanocrystalline character. In conventional zirconia ceramics, the type and composition of the alloying oxide have crucial effects both on the grain size and the stability of the tetragonal(t) phase. In this respect, oversized trivalent as well as tetravalent cation dopants and others were found to stabilize the tetragonal phase against the transformation to the monoclinic(m) symmetry. Hwang *et al*[37] found that divalent and trivalent cation additives suppressed grain growth in Y-TZP, whereas tetravalent and pentavalent cations either enhanced or did not change it. However, the microstructural evolution during sintering also depends on the solubility of the dopant, the precursor powder characteristics and the sintering conditions. In order to preserve the nanocrystalline character of the sintered ceramics, the grain growth must be inhibited either by incorporation of the second phase particles or by solid solution alloying[38].

During sintering dwell temperature and time significantly affect the grain size and final density. In order to control grain growth in a ceramic body during processing, a profound knowledge of the grain growth parameters is needed. Grain growth of zirconia alloys depends very strongly on composition and is related to the phase content. The growth of cubic grains in zirconia doped with Y^{3+} is 30-250 times faster than that of tetragonal grains alloyed with the same cation. Grain growth is strongly suppressed if both phases are coexistent. Furthermore it is well known, that Y^{3+} and Gd^{3+} suppress the grain growth very efficiently whereas Ce^{4+} does not. Up to now, the influence of a variety of alloying

elements on the grain growth has been investigated, but there is still a strong controversy about the mechanisms involved in this process[32]. Allemann *et al.*[39] measured the grain growth of differently doped zirconia materials as a function of soaking time at 1400°C. The grain size d increases with the soaking time t according to a law, best described by eqn (8):

$$d^n - d_0^n = kt \qquad \text{(eq8)}$$

Where *d* the grain size, the starting grain size d_0, the exponential parameter n, the kinetic constant *k* and the time t. The exponent n depends on the microstructure and the grain growth mechanism.

The grain growth is enhanced by doping with smaller cations. In addition, the grain growth is more effectively suppressed by large cations, if they have a lower valence state. That explains why Ce^{4+} suppresses the grain growth only weakly whereas the grain growth slows down significantly by doping with Gd^{3+} and Y^{3+}. Figure 2.10 shows a summary of the work done by Allemann *et.al* [39] for n = 3.

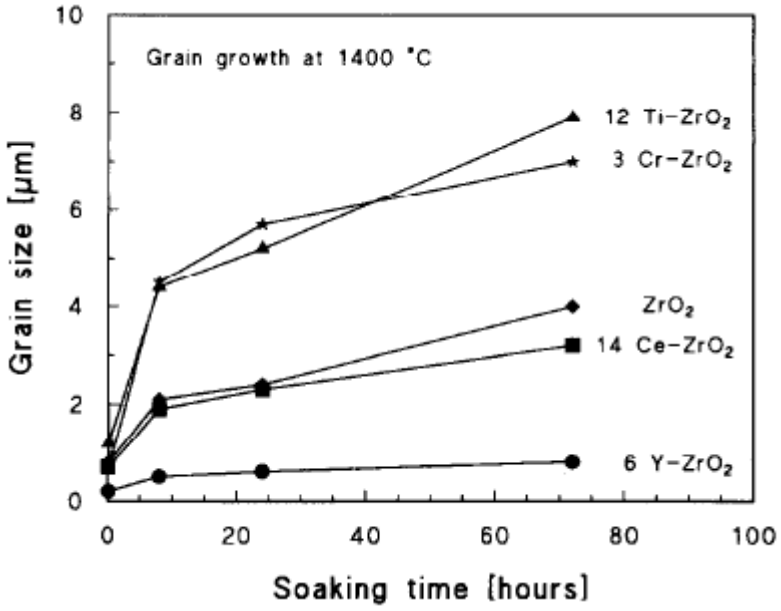


Figure 2.10: Grain sizes of differently doped zirconia as a function of soaking time at 1400°C (n = 3)[39].

Investigations of grain growth of yttria-stabilized zirconia by annealing at different temperatures were also conducted. The grain growth coefficients *k* of Y-TZP was found

to be 0.02 x 10^{-22} m^3/s , 0.12 x 10^{-22} m^3/s and 0.49 x 10^{-22} m^3/s at 1400, 1500 and 1550°C respectively doped with 6mol% Y (n = 3).

2.4.3 Grain growth mechanisms

Two models are proposed up to now.

Model 1: Theunissen *et al.*[36] proposed a solute drag model based on the observed enrichment of Y^{3+} at the surface of both Y-TZP and Y-FSZ (fully stabilised zirconia). Hwang *et al.*[40] confirmed this observation qualitatively and explained the segregation behavior of different dopants using a space charge concept.

Model 2: Based on the large differences in Y_2O_3 content from grain to grain during sluggish partitioning, Lange *et al.*[35] suggested that coherency strains arise when boundaries between grains with different compositions move, suggesting one possible correlation between sluggish phase partitioning and slow grain growth. Nauer and Carry[39] confirmed the sluggish grain growth during phase partitioning and observed an enhanced grain growth after phase segregation had occurred.

There are still some discrepancies in both of these models:

Model 1: Hwang *et al.*[40] found an enrichment factor for Y^{3+} of 1.9 whereas a much stronger enrichment factor of 4.3 has been found by Theunissen [32] . On the other hand, Nauer and Carry[39] found yttria segregation at grain boundaries only in combination with a 2 nm thick amorphous intergranular phase. The influence of such a glasslike layer on the segregation of dopants is said to be negligible by Hwang *et al.* and not taken into consideration by Theunissen.

Model 2: The most significant decrease in grain growth occurs generally with concentrations up to the solubility limit. Model 2 cannot explain the strong decrease of grain growth within the homogeneity range, as there is no compositional difference between the grains. In addition, it is difficult to explain with Model 2 the observation that the grain growth of samples within the two phase fields is approximately constant. This in spite of the fact that the compositional inhomogeneities might increase with increasing dopant concentration[39].

2.4.4. Grain growth mobility and activation energy

Grain growth may be represented by equation 9. According to the Arrhenius equation, the dependence of the kinetic constant to temperature can be described using apparent activation energy for grain growth (Q_G) as[32,41]:

$k = k_0 \exp (- Q_G/RT)$ (eq. 9)

Theunissen *et al.*[36] have studied the sintering response of ultrafine-grained 3Y-TZP ceramic prepared by chloride synthesis. They have found that the synthesized nanoscale particles were very active in sintering, but the grain growth was limited due to a solid–solution drag-controlled grain growth mechanism. Sintering characteristics of zirconia nanoceramics prepared by the sol–gel method were investigated by Maca *et al.*[32] They have shown that the sintering activation energy is half of that of submicron zirconia. Very recently, activation energy of granulated zirconia powder with the particle size <100 nm was reported by Bernard- Granger *et al*[32]. They have stated that the value of activation energy depends on the relative density.

Values of n equal to 2 and 3 give similar fits to the experimental data. Fig. 2.11 illustrates the variation in the constant k with inverse temperature for cubic, tetragonal and monoclinic zirconia, using a grain growth exponent of n = 3 (eq. 8). It is clear that the rate of grain growth in cubic zirconia is much faster than tetragonal zirconia, by about four orders of magnitude; in addition, there is a significant difference in the activation energies for grain growth[41].

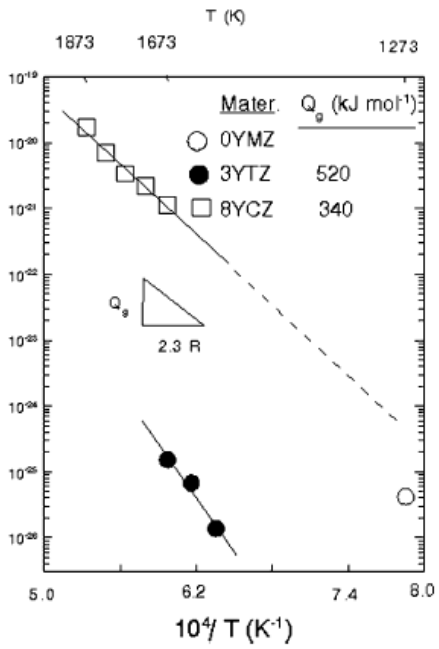


Figure 2.11: Variation in kinetic grain growth versus the inverse of temperature for cubic (8Y), tetragonal (3Y) and monoclinic (0Y) zirconia[41].

2.5. Zirconia as a biomaterial

Zirconia holds a unique place amongst oxide ceramics due to its excellent mechanical properties. This situation ensues from the considerable amount of research work done since the discovery of the transformation toughening abilities of zirconia. The recent introduction of zirconia-based ceramics as restorative dental materials has generated considerable interest in the dental community. Biomedical grade zirconia was introduced during the 1980's as a solution to alumina brittleness and the consequent failure of these implants[11,42,43]. As of 2006, more than 600 000 femoral heads have been implanted worldwide, mainly in the USA and Europe.

Biomedical grade zirconia falls under the TZP category of zirconia ceramics and exhibits the best mechanical properties of the oxide ceramics: this is the consequence of phase transformation toughening, which increases its crack propagation resistance. Table 2 shows the mechanical properties of biomedical grade zirconia[52].

The stress-induced phase transformation involves the transformation of metastable tetragonal grains to the monoclinic phase at the crack tip, which, accompanied by volume expansion, induces compressive stresses[42].

Alumina and zirconia ceramics are often considered bio-inert since no material-bone interface is created. The soft tissue interlayer always shields the bone from the implant. This biological shielding unfortunately leads to mechanical (stress) shielding, known to promote micro-motion and subsequent aseptic implant loosening. Only under compression, with a porous structure and with a good fit with bone cavity (avoiding relative micro-motion), the fibrous tissue at the interface is thin enough and a successful bone in-growth is achieved. Given these restrictions, bio-inert ceramics are hardly used as bone fillers. Their major application in orthopedics concerns total hip and knee replacement. The use of bio-ceramic materials reduces wear rates of bearing components and produces negligible amount of ion release[42,43].

Biomedical grade zirconia usually contains 3mol% yttria (Y_2O_3) as a stabilizer (3Y-TZP). 3Y-TZP has been used to manufacture femoral heads in total hip replacement prostheses since the late eighties and is currently available in dentistry for the fabrication of dental crowns and fixed partial dentures. Dental applications add aesthetic requirements (colour, translucency) to the mechanical specifications. White to ivory colour gives a clear advantage for oxide ceramics versus metals, which is the reason why research and development are nowadays directed towards metal-free dental prosthetic restorations[11,26,42,43]. Translucency of technical ceramics may be achieved with a very fine (submicron) grain size and low porosity content (less than 1%). Fully dense, translucent (3mol% yttria-stabilised) zirconia ceramics can be processed with small equiaxed grains of size 0.2-0.5 μm in diameter and meet the demand for both natural-teeth-looking restoration and high mechanical strength[11,43]. For the last 10 years 3Y-TZP has been considered the ideal solution for dental material. Figure 2.12 represents a micrograph of biomedical grade zirconia:

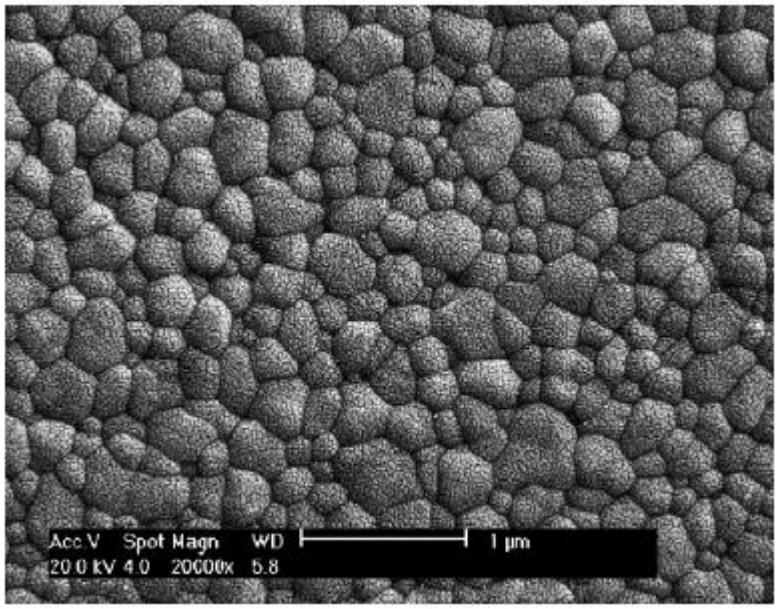


Figure 2.12: Microstructure of Bio-medical grade zirconia for dental applications[11].

Currently available 3Y-TZP for soft machining of dental restorations utilize final sintering temperatures varying between 1350 and 1550°C depending on the manufacturer. This fairly wide range of sintering temperatures is therefore likely to have an influence on the grain size and later the phase stability of 3Y-TZP for dental applications. From the phase diagram established by Scott[10], 3Y-TZP contains some amount of cubic zirconia. Chevalier *et al.*[43] demonstrated that the presence of cubic zirconia is not desirable in 3Y-TZP for biomedical applications and is caused by the uneven distribution of the yttrium stabilizer ions. The cubic grains are enriched in yttrium while the surrounding tetragonal grains are depleted and therefore less stable.

Chapter 3: Experimental Procedure

This section describes the experimental procedures, equipment, raw materials and chemicals used in this presented work. Where necessary, outlines of the equipment functions and how the analysis was conducted are given.

3.1. Ceramic Preparation

3.1.1 Powder Preparation Method

Powders used in this study were prepared via a particular co-precipitation method. Solutions of 100g $ZrOCl_2.8H_2O$ and 3.431g YCl_3 were dissolved in 1 L water at 80°C under stirring in the correct ratio to produce a 3 mol% yttria stabilised tetragonal zirconia powder (3Y-TZP). NH_3 solution was then added drop-wise to the rapidly stirring zirconia mixture. A gelatinous mass starts to precipitate from pH ≈ 4, but all zirconium is precipitated at pH = 9. The resulting precipitate was then washed with distilled water and propanol three times. The precipitate was then oven-dried at 100°C overnight. Subsequently the dried product was ground using a pestle and mortar in order to break down the hard lump-like structures. The powders were then calcined in air as discussed below. For comparison purposes commercial 3Y-TZP powders were also used for this project. The precursors used in the preparation of the powders as well as the commercial powders are all given in table 3.1:

Table 3.1: Chemicals used in the co-precipitation method

Chemical	**State**	**Source**	**Purity**
3 mol% Yttria stabilised zirconia	Solid	Geratech Zirconium Beneficiation Ltd	-
Zirconium oxychloride hexahydrate	Solid	Geratech Zirconium Beneficiation Ltd	-
Anhydrous yttrium chloride	Solid	Sigma Aldrich	99.9%
Ammonia	Liquid	Chemical Stores-Wits University	25%in solution
2-propanol	Liquid	Chemical Stores-Wits University	99.0%

3.1.2 Calcination

After preparation, the powders still contain adsorbed solvent as well as water and other volatile impurities[23]. In addition, the oxide is still present in an amorphous state and the crystalline solid solution has not yet been formed. In order to remove the volatile impurities and crystallize the powder, it is necessary to subject the powder to heat treatment, i.e. *calcination.* Dried ZrO_2 powders were calcined at 600°C, 700°C, 800°C, 900°C, and 1000°C respectively to determine the appropriate calcination temperature. Heating and cooling rates of 5°C/min were used and a dwell time of 1 hour was chosen unless otherwise stated. High temperatures and long dwell times can cause excessive particle growth and hard agglomerate formation which can be detrimental to the final product. The calcined powders were qualitatively and quantitatively characterized by XRD for phases present.

3.1.3 Milling

After calcination, a certain amount of agglomeration normally occurs, which is detrimental to the final product. In order to break down the agglomerates and to obtain a

powder which will compact and sinter uniformly to a high density, it is necessary to mill the powder. For this study an attritor mill was used after calcination. This consists of an alumina paddle and pot. 20g of powder is suspended in 350cm^3 of isopropanol and approximately 400g of zirconia milling balls (1mm in diameter) are added. The paddle was rotated at 300rpm. After milling the powder is dried using a rotary evaporator.

3.1.4 Particle Size Analysis

After milling for a specific amount of time 10cm^3 of the zirconia solution was mixed with 80cm^3 of 0.25 % solution of tetra-sodium-pyrophosphate anhydrous and the resulting solution was analyzed using a Micrometrics Sedigraph III instrument at the Geratech premises. The powder was sonicated for 1 minute.

3.1.5 Binder Addition

To aid the subsequent processes, 3% (m/m) of PEG 400 solution was added to the dried powder in a turbula mixer and mixed for 2 hours.

3.1.6 Compaction

After milling, it is necessary to form the powder into shapes suitable for sintering and subsequent mechanical testing. Approximately 2g of powder were compacted uniaxially using a cylindrical piston die at a pressure of 250MPa at room temperature and held for 60 s. The resulting pellets were about 18mm in diameter and 3mm thick and referred to as green bodies.

3.1.7 Binder burnout

The green bodies were all heated up to 400°C to remove the binder. This was done in a furnace in air at a heating and cooling rate of 5°C/min. The samples were kept at 400°C for an hour to remove the binder.

3.1.8 Sintering

Sintering was performed in a muffle furnace in air for all samples. The sintering temperatures used were 1150°C, 1250°C, 1350°C, 1450°C, and 1500°C.

In order to achieve dense zirconia-based materials, it is necessary to use high heating rates to suppress grain boundary diffusion at lower temperatures and promote bulk diffusion at higher temperatures[35].

The green bodies were heated to the sintering temperature at a rate of 5°C/min where samples were held for two hours before cooling down to room temperature at a rate of 5°C/min. Figure 3.1 below shows a schematic of the preparation process:

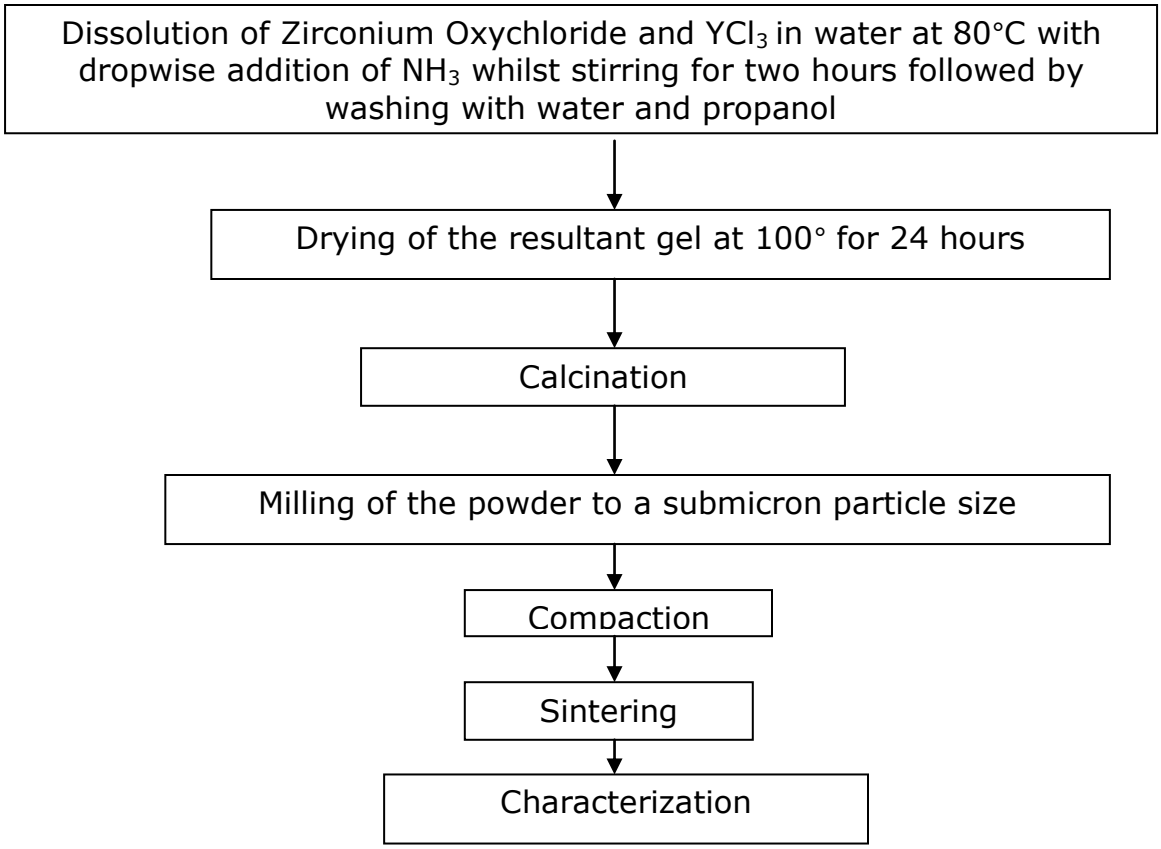


Figure 3.1: Schematic of the preparation process for the zirconia ceramic

3.2. Ceramic Characterization

3.2.1 Density Measurements

The density of the green compacts were calculated from the measured mass and geometrically determined volume, while the density of the sintered samples were determined using the Archimedes technique. The sintered samples were boiled in water for three hours in order to fill the pores with steam. The samples were then left to cool to ambient temperature. The mass of the sample suspended in water was then determined (m_s), followed by the water-saturated mass (m_w). M_w was done by drying the surface of the sample with a paper towel then determining its mass. Five readings were taken for each mass (both m_s and m_w) and then an average taken. The samples were then dried in an oven at 100°C for 20 minutes and this dry mass was measured (m_d). Density values were obtained from an average of three samples. The density and open porosity was calculated using the equations 3.1 and 3.2[30]:

$$\rho_s = \frac{m_d \rho_{water}}{(m_s - m_w)} \qquad \text{(eq. 3.1)}$$

$$P_o = \left(\frac{m_w - m_d}{m_w - m_s} \right) \times 100 \qquad \text{(eq. 3.2)}$$

where ρ is the bulk density (g/cm^3); m_d is the dry mass (g); m_s is the mass of the samples suspended in water (g); m_w is the water saturated mass (g); and ρ_{water} is the density of water (g/cm^3); and P_0 is the percentage open porosity.

3.2.2 Thermal etching

Thermal etching is a technique that reveals the higher energy associated with the grain boundaries of a material. All the samples were thermally etched for 20 minutes at a temperature 50°C below the sintering temperature prior to SEM measurements.

3.2.3 Vickers Hardness

Vickers hardness values were measured on polished surfaces using a Vickers hardness diamond indenter at a 10kg load held for ten seconds. The hardness values were obtained from an average of four indents on each of the three samples.

The equation from which the Vickers hardness is derived is shown below:

$H_v = 1.854 \times P/a^2$ (eqn. 3.3)

where H_v is the Vickers hardness; P is the indentation load (kg); and a is half the indentation diagonal (mm).

3.2.4 Indentation Fracture Toughness

The measurement of a ceramic's fracture toughness is not straight forward. A number of techniques may be employed which often lead to varying results. The fracture toughness of sintered specimens was determined by the indentation-fracture method performed under the nominal applied load of 98.1 N. Because zirconia cracks in a Palmqvist, rather than a half-penny mode[44], the fracture toughness was obtained from the expression given by the Shetty equation[46]:

$K_{ic} = 0.0889 (HP/4L)^{0.5}$ (eqn 3.4)

where again H and P are the Vickers hardness and indentation load respectively, L = c –a; 2a the indentation diagonal and 2c the length of the full crack (both in m).

For the equations above, the crack lengths were measured immediately after the indentation was carried out in order to av crack growth after removing the load.

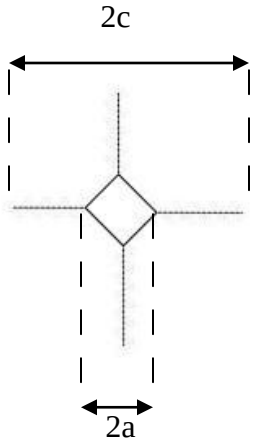


Figure 3.2: Schematic of the Vickers hardness indentation showing the radial cracks produced by the diamond indentor.

3.2.5 Scanning Electron Microscopy (SEM) and Grain Size Determination

SEM was used to investigate the microstructure of the zirconia samples. Grain size measurements were undertaken from the micrographs of polished, thermally etched samples and an average taken using the linear intercept method. A Phillips XL-30 SEM ESEM-FEG scanning electron microscope equipped with a field emission gun operating between 8-20kV was used to assess the microstructure of the polished samples. The samples were put on a carbon tape and mounted on the stage of the microscope. Secondary electrons were used to take images at a voltage of 10.0kV and a magnification range of 1000x-20000x at various spots. The etched samples were coated with gold using a gold-sputterer before being placed on the carbon tape. The SEM is coupled to an Energy Dispersive X-ray Spectrometer (EDS) which can provide rapid qualitative, or with adequate standards, quantitative analysis of elemental composition with a sampling depth of 1-2 microns.

3.2.6 X-ray Diffraction

The Philips 1710 Diffractometer, equipped with a graphite monochromator and a copper anode using K_α as the radiation. The X-ray tube was operated at 40kV and 20mA at a wavelength of 0.154 nm.The scanning range was 10 - 70° (2θ) using the step size of 0.02° and 0.50 seconds per step. Patterns were collected and phase identification was done using X'Pert HighScore software containing ICDD (International Centre for Diffraction Data) data files for comparison.

Phase quantification and crystallite size was done using the Eva Software with the assistance of Professor Billing in the Chemistry Department at the University of Witwatersrand.

3.2.7 Thermal Analysis

Two thermal analysis techniques were used for powder characterization: Differential thermal analysis (DTA) and thermogravimetric analysis (TGA). DTA was used to identify the regions for the removal of unreacted adsorbed organic molecules, crystallization, and tetragonal to monoclinic transformation. The experiments were carried out to 1500°C with heating and cooling rates of 10°C/min.

TGA was used to identify the temperature regions for the removal of unreacted organic solvents and this is represented by mass loss. The experiments were carried out to a 1000°C, with heating and cooling rates of 10°C/min. A Setaram TGA 92 was used for the DTA/TGA analysis.

3.2.8 Three-point bend test

Measurement of flexural strength was performed using a three-point bending jig with 15mm between the supports. The specimens were loaded in the middle until fracture.

The crosshead speed was 1mm/min and load at fracture was recorded. The flexural strength (*M*) in megaPascals (MPa) was calculated according to the following equation:

$$M = 3Wl/2bd^2 \qquad \text{(eqn. 3.5)}$$

where *W* is the load at fracture in Newtons (N), *l* the test span (centre-to-centre distance between the supporting rollers), *b* the width of the specimen, and *d* is the thickness of the specimen, all measured in millimetres (mm)[47]. Due to equipment and time limitations, samples with dimensions 15x2x1mm were obtained by compacting Geratech powders at 11 MPa at the Multotec premises and subsequently sintered. The sintered specimens were then cut, ground, and polished to the required dimensions which are half the size prescribed by the ISO 14704:2000 standard[50]. Three samples were tested at each of the sintering temperatures.

Chapter 4: Results

In this section the results obtained are reported. The chapter is divided into three main parts:

- Characterization of the Geratech powder and the mechanical properties of the sintered ceramic respectively;

- Characterization of the co-precipitated powder, their sintering behavior and the mechanical properties of the sintered ceramic respectively;

- Sintering and characterization of the commercial Wieland Zeno Zirconia discs (appendix 3).

4.1. The Geratech powder

4.1.1. X-ray diffraction data of the Geratech powder

Yttria stabilised as well as monoclinic zirconia powder supplied by Geratech were characterized by SEM, EDS, and XRD together with Rietveld refinement. This was done to compare the commercial powder to the powder synthesized as described in section 3.1.1. Figures 4.1 and 4.2 below show the XRD patterns of the monoclinic and yttria stabilised powder supplied by Geratech respectively, where m = monoclinic and t = tetragonal.

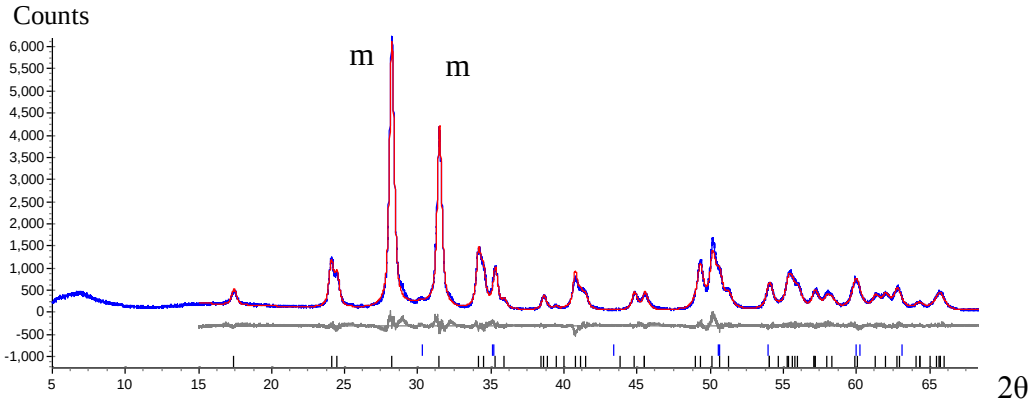


Figure 4.1: XRD data for the monoclinic zirconia powder supplied by Geratech.

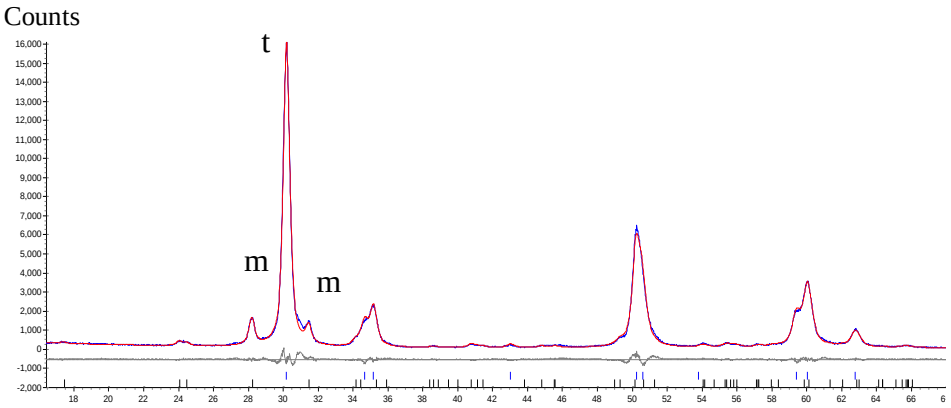


Figure 4.2: XRD pattern of the 3 mol% yttria stabilised powder supplied by Geratech

Table 4.1 shows the results of the Rietveld refinement analysis with regards to phase quantification and crystallite size.

Table 4.1: XRD data for the Geratech powders

Powder	**Phases from the XRD**	**Crystallite size (nm)**
Monoclinic ZrO_2	Monoclinic: 95% Tetragonal: 5%	Monoclinic: 75.8 ± 3.3 Tetragonal: 12.8 ± 5.8
Yttria Stabilised ZrO_2	Monoclinic: 15% Tetragonal: 85%	Monoclinic: 40.5 ± 4.7 Tetragonal: 53.6 ± 2.5

XRD patterns were obtained on the monoclinic and yttria stabilised zirconia commercial powders supplied by Geratech Ltd to determine the phases present both qualitative and quantitatively and the crystallite sizes.

The crystallite sizes are in the nanometer range which explains the broadness of the peaks in the XRD patterns. Peak broadening is usually associated with crystallite sizes in the nanometer range. The monoclinic powder (table 4.1) shows the existence of two phases, monoclinic and traces of tetragonal. This implies that the particle size is small enough for the tetragonal phase to be metastable without the addition of yttria or due to an internal scheme of tetragonal inclusions in the monoclinic particles. According to Chen *et al.*[25] to stabilise the tetragonal phase without the addition of a stabilizing agent, the

particle size has to be approximately 20-30nm. This is consistent with the particle size of the tetragonal phase of 12.8nm (table 4.1).

The XRD pattern of the stabilised powder (fig. 4.2) consisting of a 3 mole % yttria stabilizing agent shows an 85% tetragonal phase. The presence of the monoclinic phase shows that there was sufficient grain growth during the calcination process to favour a small amount of t-m transformation during cooling as shown by the relatively low intensity of the monoclinic peaks. As shown in table 4.1 the crystallite sizes are very fine with sizes ranging from approximately 40-60nm corresponding to the broad peaks shown in the XRD pattern in fig. 4.2.

4.1.2. SEM of the powders supplied by Geratech

SEM micrographs (all in secondary electron mode) were obtained on the powders supplied by Geratech to determine the morphology and particle size of the powder.
Figure 4.3 below shows a micrograph of the monoclinic powder supplied by Geratech. The micrograph shows agglomerates made up of very fine spherical primary particles. The primary particles can be seen to be under 1μm into the nanometer range which is consistent with the XRD results displayed in table 4.1 and figure 4.1.

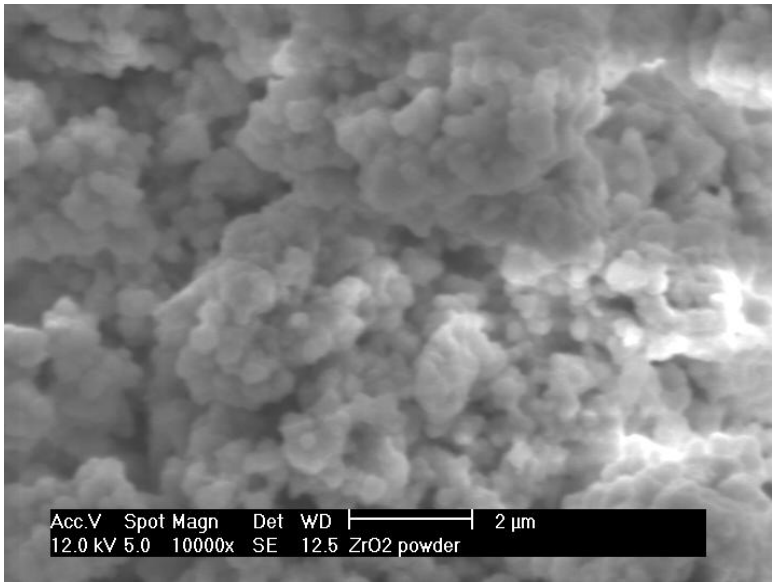


Figure 4.3: SEM micrograph of the monoclinic powder supplied by Geratech

Figure 4.4 below shows the micrograph of the 3 mole% yttria stabilised zirconia supplied by Geratech. The micrograph shows agglomerated particles made up of very fine spherical primary particles in the nanometer range which is consistent with the XRD results shown in table 4.1.

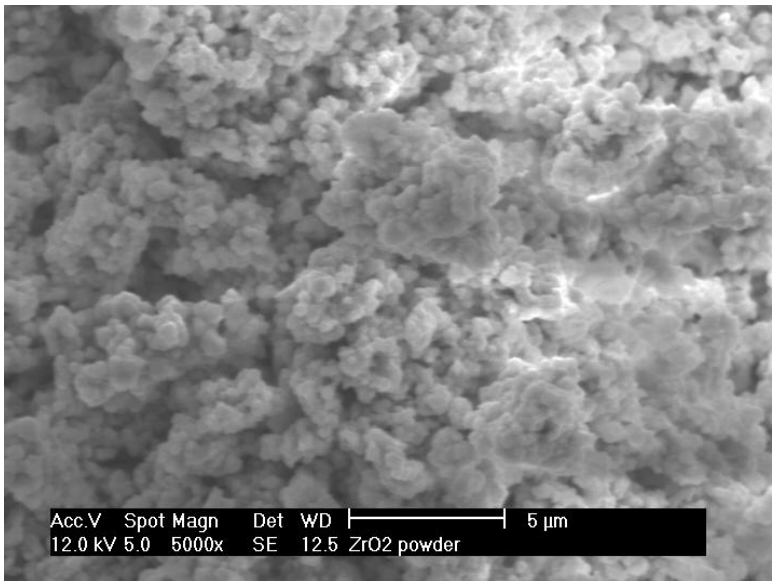


Figure 4.4: Micrograph of 3Y-zirconia supplied by Geratech

4.1.3. Particle size analysis of the 3 mol% Yttria stabilised Zirconia powder supplied by Geratech Ltd

The 3 mol% yttria stabilised zirconia powder supplied by Geratech contains a certain amount of agglomeration. It was therefore necessary to mill the powder in order to achieve a powder that would compact and sinter uniformly to a high density (section 3.1.3). After milling, the powder was then sonicated for 1 minute (section 3.1.4). Figure 4.5 shows the particle size distribution of the stabilised powder prior to milling supplied by Geratech where d_{10} = 10 percentile, d_{50} = median, d_{80} = 80 percentile.

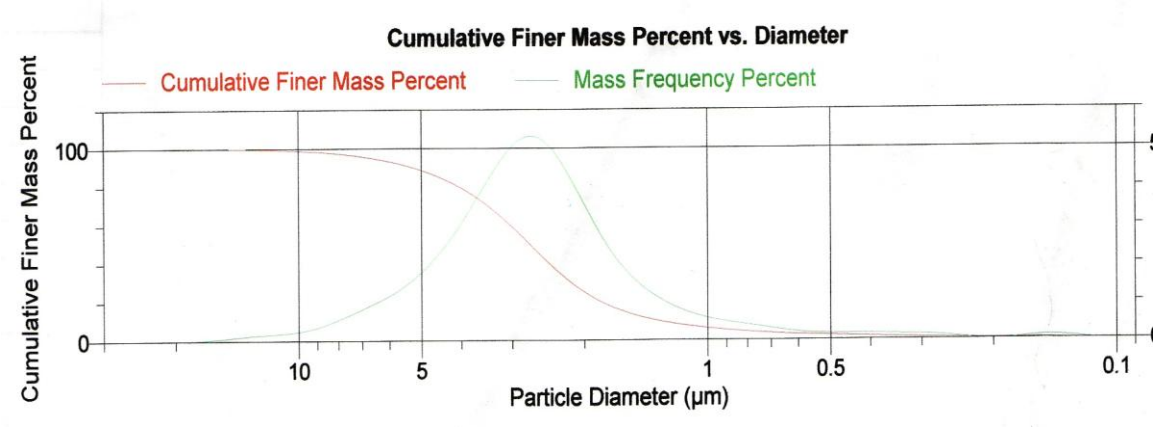


Figure 4.5: Particle size distribution of the initial powder supplied by Geratech Ltd

The percentiles were as follows: d_{10} = 1.31 µm; d_{50} = 2.41 µm; d_{80} = 4.02 µm.

From figure 4.5 the yttria stabilised powder supplied by Geratech shows a monomodal particle size distribution displaying a single peak with maximum at 2.41µm. This correlates with the SEM micrograph in figure 4.4 which shows agglomerates made up of very fine primary nano-particles. Due to the strength of these agglomerates the particle size distribution reflects the size of the agglomerates even after sonication.

After milling for approximately 10 hours at 300rpm, the particle size was reduced significantly as shown in figure 4.6:

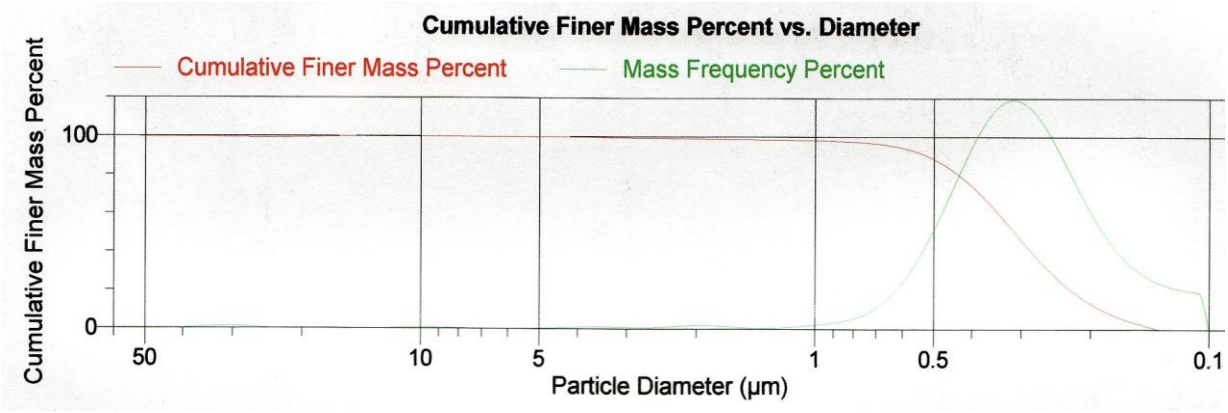


Figure 4.6: Particle size distribution of the yttria stabilised zirconia supplied by Geratech after 10 hours of milling

The percentiles were as follows: d_{80} = 0.43µm; d_{50} = 0.30µm; d_{10} = 0.19µm.

Figure 4.6 shows a monomodal particle size distribution displaying a single peak at the maximum of 0.30µm. This was thought to be sufficient for the subsequent compaction and sintering processes.

Table 4.2 shows the effect of milling time on the particle size:

Table 4.2: Effect of milling time on particle size distribution of the 3 mole% yttria stabilised zirconia powder supplied by Geratech.

Time (hours)	**Particle size (d_{10})**	**Particle size d_{50} (µm)**	**Particle size (d_{90})**
0	1.31 ± 0.35	2.41 ± 0.86	4.02 ± 1.01
2	1.00 ± 0.23	1.37 ± 0.44	2.34 ± 0.77
4	0.64 ± 0.27	1.01 ± 0.12	1.50 ± 0.33
6	0.33 ± 0.30	0.77 ± 0.35	0.99 ± 0.53
8	0.25 ± 0.46	0.58 ± 0.11	1.79 ± 0.88
10	0.19 ± 0.33	0.30 ± 0.20	0.43 ± 0.33
12	0.24 ± 0.43	0.43 ± 0.12	0.63 ± 0.15

As can be seen in table 4.2, the particle size decreases as milling time increases. The particle size drops significantly in the beginning (0-2 hours) and then decreases more steadily as time progresses until it reaches a minimum of 0.3µm. After 10 hours, the

particle size levels off showing that the agglomerates are too strong to further break down.

4.1.5. Compaction of the yttria stabilised zirconia powder supplied by Geratech.

Usually complete densification in the sintered compact is obtained for high degree of homogeneity of the packing green compact. This is linked to the nature of the powders and may be achieved when powders have small crystallites size and are unagglomerated. Figure 4.7 below shows the compaction graph of the yttria stabilised powder supplied by Geratech. This was done in order to achieve a high green density and subsequently high densification during sintering.

3 wt% PEG 400 was mixed with the powder using a turbula mixer prior to compaction. For this project a compaction pressure of 250 MPa was used at a holding time of one minute in order to achieve a green density of approximately 50%. At higher pressures there is no significant increase in density.

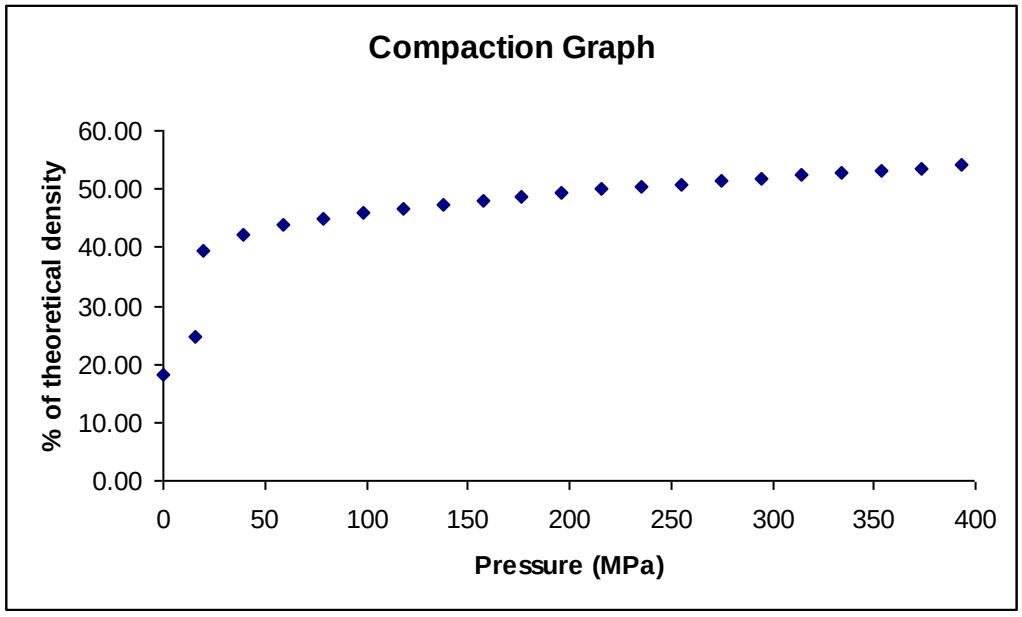


Figure 4.7: Compaction curve of the yttria stabilised powder supplied by Geratech

The compaction plot shows the density as a function of the applied pressure. From a pressure of 0 MPa to approximately 20 MPa there is a significant increase in relative

density and is consistent with the rearrangement of agglomerates in the die. This stage is caused by the friction between the particles until they are on fixed positions relative to each other[49]. After this region the curve sees a less significant increase in relative density with increasing pressure and corresponds to an elimination of the interagglomerate porosity[49].

4.2. Characterization of the sintered ceramic

After compaction the green bodies were sintered at various temperatures to find the temperature that would best optimize the mechanical properties. The temperatures used were 1150°C, 1250°C, 1350°C, 1450°C and 1500°C for two hours. The resulting sintered ceramic was characterized by the Archimedes density technique, XRD, and SEM.
XRD patterns and SEM micrographs were obtained on the sintered samples to determine the phases present, the microstructure, and the grain size. Unfortunately due to poor electron conduction even after coating, some SEM images were not taken for some of the samples.

4.2.1. Densities and grain sizes of the ceramic after sintering

Table 4.3 shows the density and grain size of the sintered ceramic after sintering for two hours at various temperatures. Densities and open porosities were determined by the Archimedes technique and the average grain size was determined using the linear intercept method for samples where possible.

Table 4.3: Densities of the sintered ceramic as a function of temperature sintered for two hours

Sintering temperature	**Density (g/cm^3)**	**%Open porosity**	**%Theoretical density***	**Average grain size (μm)**
1150	**5.05**	**14.5**	**83.6**	**-**
1250	**5.83**	**2.3**	**96.5**	**0.16 ± 0.02**
1350	**6.04**	**0.0**	**100**	**0.19 ± 0.01**
1450	**6.00**	**0.5**	**99.3**	**0.30 ± 0.02**
1500	**5.92**	**1.90**	**98.0**	**-**

*****Theoretical density[29] = 6.04 g/cm^3. Reference [52] states that biomedical grade zirconia has a density > 6.00g/cm^3.

4.2.2. SEM Micrographs of the ceramic sintered at various temperatures

Figure 4.8 below shows the SEM micrographs of the ceramic sintered at various temperatures. The samples were thermally etched for 20 minutes at temperatures 50°C below the sintering temperature.

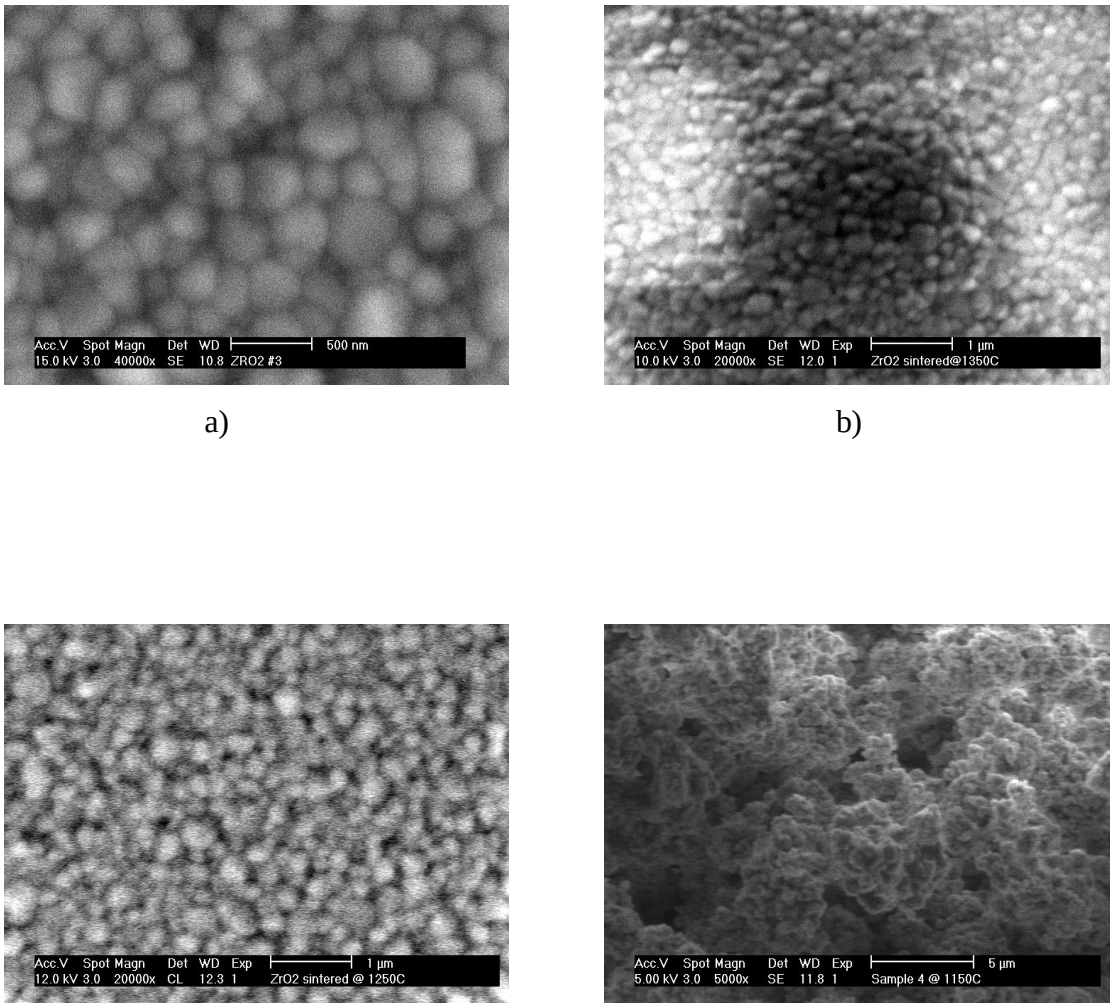
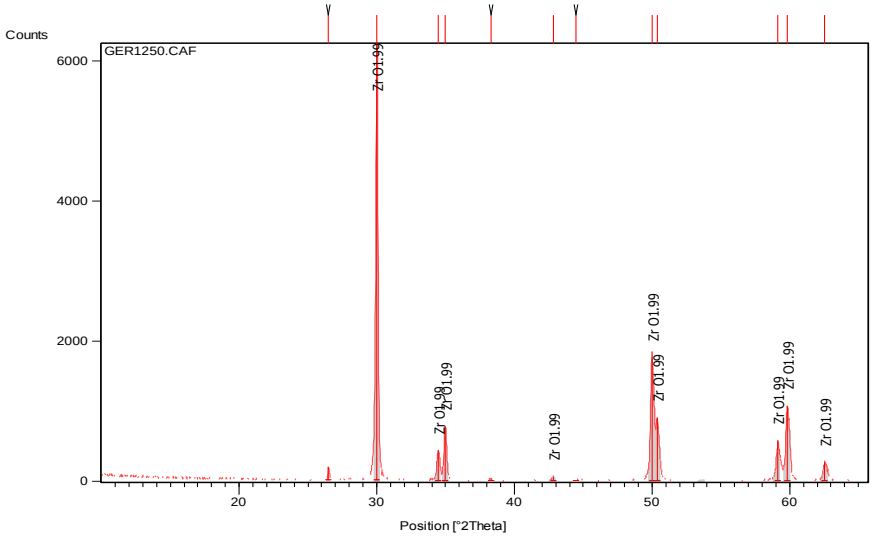


Figure 4.8: SEM micrographs of the ceramic sintered at: a) 1450°C; b) 1350°C; c) 1250°C; d) 1150°C, for two hours.

4.2.3. XRD patterns of the ceramic sintered at various temperatures

Figure 4.9 below shows the XRD patterns of the ceramic sintered at various temperatures. It shows the predominant presence of the tetragonal phase with some monoclinic phase.

a)



b)

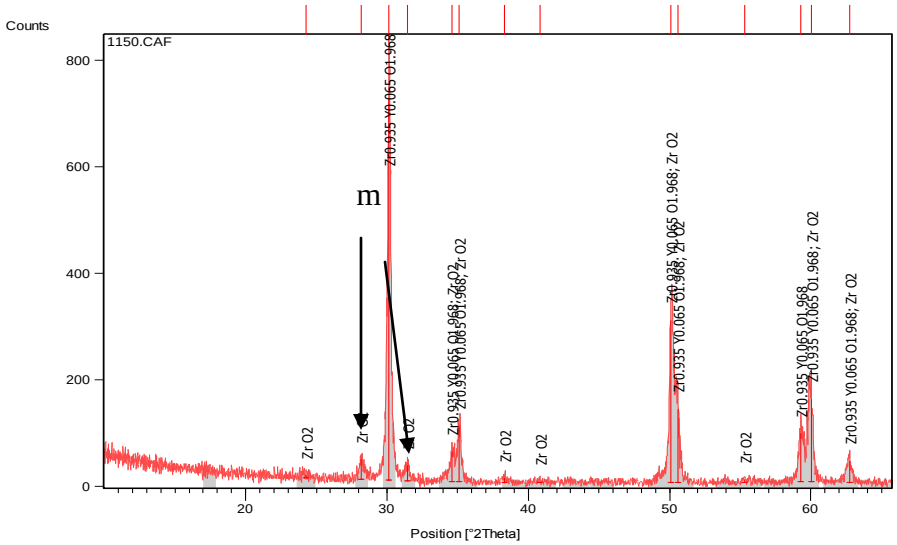


Figure 4.9: XRD patterns of the ceramic sintered at temperatures a) 1250°C; b) 1150°C. m = monoclinic phase. The rest of the peaks are tetragonal.

SEM micrographs and XRD patterns were taken of the ceramic sintered at various temperatures to obtain the phases present and the microstructure. All the SEM micrographs regardless of sintering temperature consist of small equiaxed grains of approximately 0.1-0.5μm in diameter. The samples sintered at 1450 and 1350°C (fig. 4.8) consists of small densely packed equiaxed grains consistent with the microstructure required for biomedical grade zirconia. The sample sintered at the lower temperature of 1250°C (fig. 4.8) also consists of small grains however the materials are not as dense as those sintered at the higher temperatures. Porosity can be detected in the sample sintered at 1250°C using the Archimedes density method. The XRD pattern for the sample sintered at 1250°C and above shows a fully stabilised tetragonal structure. The sample sintered at 1150°C (fig 4.8) shows lower densification. This indicates that 1150°C is not a high enough temperature to achieve high densification. This is confirmed in the Archimedes density measurements. The XRD pattern (fig. 4.9) shows the retention of some of the monoclinic phase indicating and confirming that 1150°C is not a high enough sintering temperature.

4.2.4. Mechanical properties of the sintered ceramic from the 3Y-zirconia powder supplied by Geratech

Mechanical testing such as hardness, indentation fracture toughness and density, were performed on the ceramic after being sintered at the various temperatures as described above. Table 4.4 shows a summary of the mechanical properties.

Table 4.4: Summary of the mechanical properties of the sintered ceramic at various temperatures

* The cubic phase may be present but it is very hard to distinguish between the t and c phases without vibrational spectroscopy[17,34]. Due to this the original theoretical density below is still assumed since the target density is 6.00g/cm^3 or greater.

**theoretical density[29] = 6.04 g/cm^3

Sintering temperature (°C)	Sintered density (% theoretical)**	Phases present From the XRD	Hardness (GPa)	Fracture Toughness (MPa.m$^{0.5}$)
				Shetty[46]
1150	83.6	m, t	7.2 ± 0.8	5.4 ± 0.1
1250	96.5	t	11.1 ± 0.1	5.8 ± 0.1
1350	100	t	13.5 ± 0.2	6.0 ± 0.0
1450	99.3	t	13.0 ± 0.1	6.4 ± 0.3
1500	98.0	t, c*	12.4 ± 0.3	6.2 ± 0.1

The relative densities of the samples generally increase with increasing temperature but drops at 1500°C due to the possible formation of the cubic phase[34]. Hardness values increases with increasing sintering temperature and density however the hardness for the sample sintered at 1350°C is higher than the hardness of the sample sintered at 1450°C and this can be attributed to the grain size effect as described by the Hall-Petch equation[48].

The indentation fracture toughness increases with increasing temperature until 1450°C where it drops at 1500°C. This again may be due to the presence of the cubic phase as discovered by Lange[35] which is non-transformable[21,22]. Other explanations include the presence of the monoclinic phase as in the sample sintered at 1150°C as well as the presence of the critical grain size as discussed in the literature review (section 2.4.1) and further discussed in section 5 (Discussion).

4.3. The co-precipitated powder

The powders discussed in this section were prepared via the co-precipitation route as described in section 3.1.1 and characterised by DTA/TGA, SEM, EDS, XRD together with Rietveld Refinement.

4.3.1. DTA/TGA results of the prepared powder

On the basis of the ZrO_2-Y_2O_3 phase diagram, 3 mol% yttria-stabilised zirconia was prepared as mentioned in section 3.1.1. The powder was then subjected to thermal treatment.

Typical DTA and TGA curves of the yttria-stabilised zirconia powder are shown in figure 4.10. The blue trace (DTA) shows heat flow from and to the sample, indicating endothermic and exothermic reactions. The green trace is the mass loss during heating (TGA). Three main stages can be distinguished during heating. The first occurs at the temperature range of 100°C - 220°C. This corresponds to the loss of adsorbed water and solvents. The second stage is between 220°C and 400°C which corresponds to the loss of bonded water and organics. A further 5% of mass loss corresponds to the removal of the last OH^- group up to a 1000°C. The crystallization peak was expected to occur below 600°C (confirmed by the XRD pattern in figure 4.13) where the powder crystallizes (from an amorphous state) but the process is too slow therefore the peak is not visible. The exothermic peak representing the t-m transformation is not seen during cooling. This confirms that the powder is indeed the tetragonal (metastable) structure.

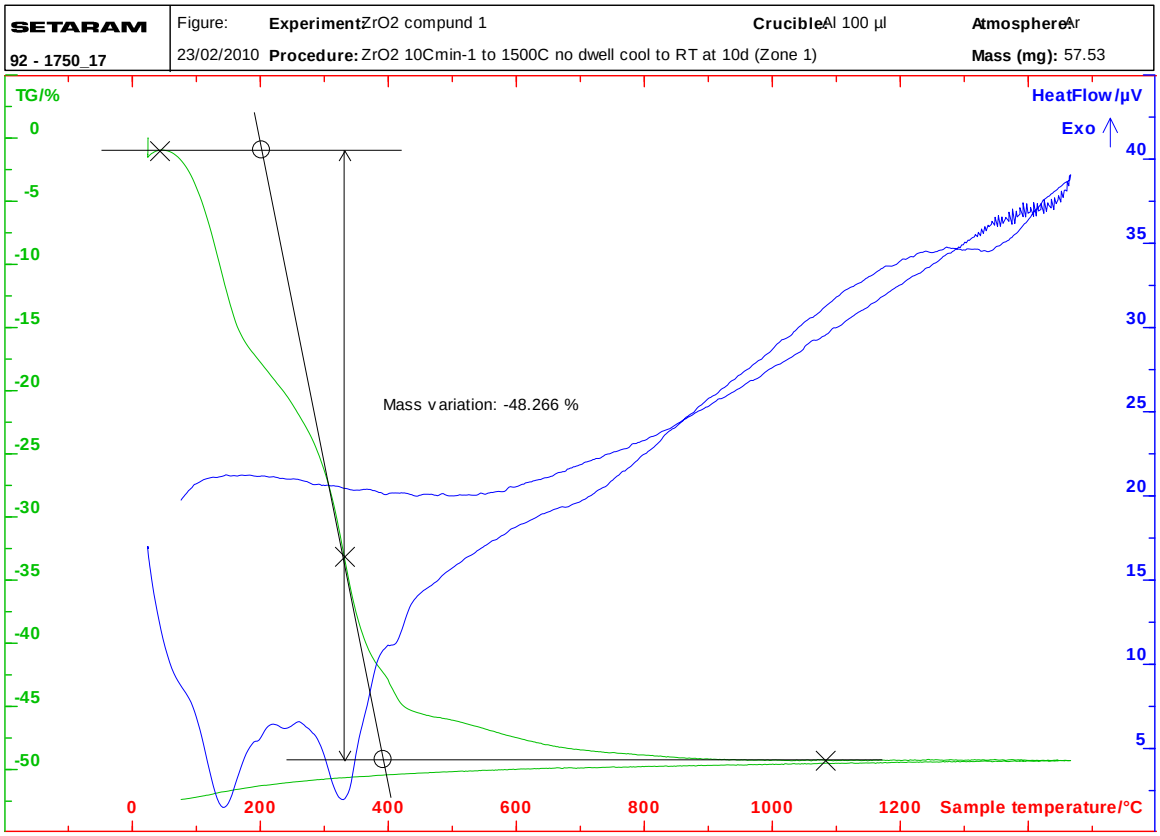


Figure 4.10: DTA/TGA trace of the uncalcined 3Y-zirconia prepared via the co-precipitation route.

4.3.2. Calcination of the co-precipitated powders

The prepared 3 mol% yttria stabilised ZrO_2 powders were calcined at 600°C, 700°C, 800°C, 900°C, 1000°C for one hour. The calcined powders were then characterized using XRD together with Rietveld Refinement, SEM and EDS. Figure 4.11 shows the XRD pattern of the powders calcined at various temperatures:

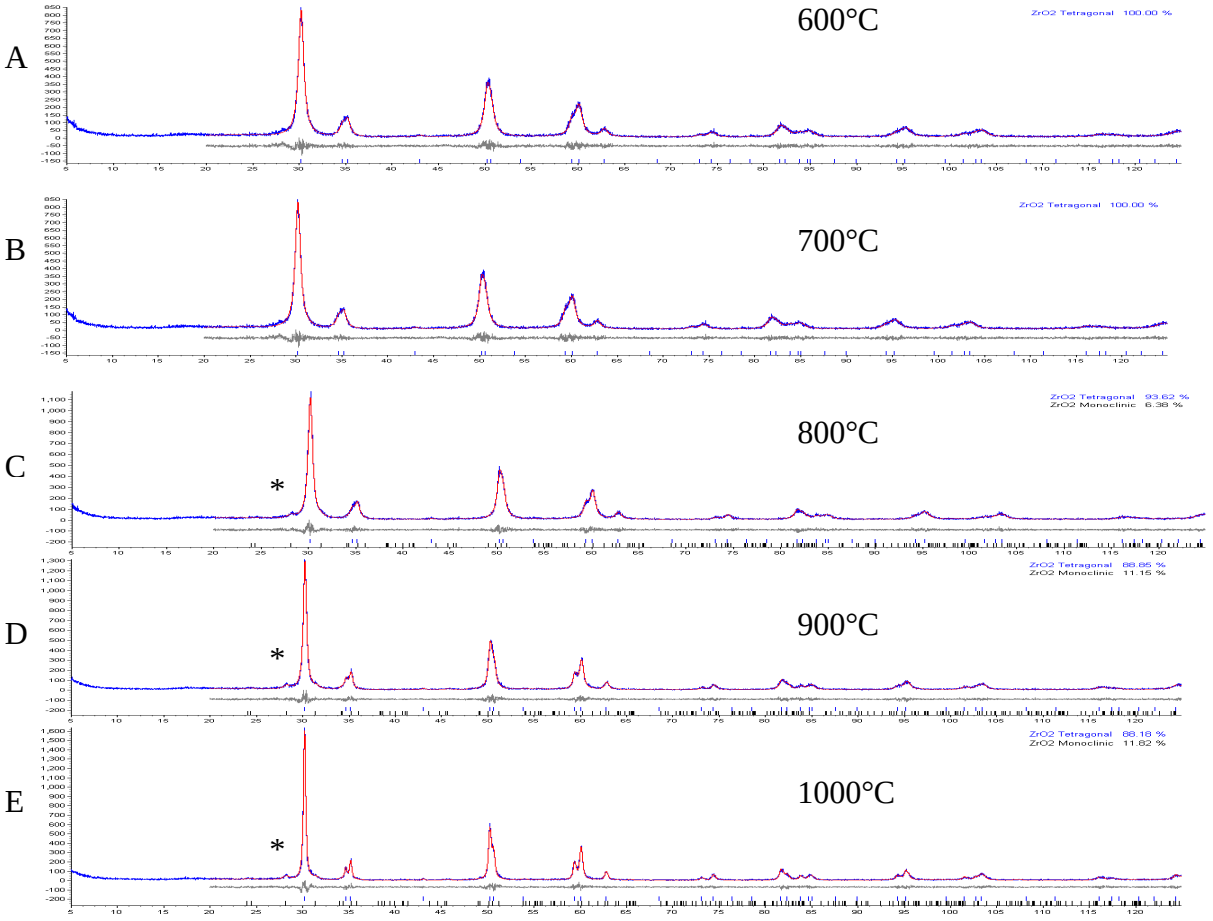


Figure 4.11: XRD pattern of powder calcined at various temperatures; A = 600°C, B = 700°C, C = 800°C, D = 900°C, E = 1000°C
* = monoclinic phase, all other peaks are tetragonal

At 600°C the powder is already crystalline and in tetragonal form. With increasing temperature the powder becomes more crystalline until 800°C where the monoclinic phase starts to appear. The appearance of the monoclinic phase indicates that from 800°C upwards there is a modest amount of grain growth to favour a small amount of t – m transformation upon cooling as indicated by the low intensity of the monoclinic peaks in fig 4.11C. Table 4.4 shows the quantity of phase present as well as the crystallite size of each of the powder:

Table 4.5: XRD data of the 3Y-ZrO_2 powder obtained after various thermal treatments for one hour

Calcination temperature (°C)	**Phases from the XRD**	**Crystallite Size (nm)**
600	Crystalline Tetragonal phase: 100%	9.9 ± 0.1
700	Crystalline Tetragonal phase: 100%	13.6 ± 0.1
800	Crystalline Tetragonal phase: 93.6% Monoclinic phase: 6.4%	Tetragonal: 17.2 ± 0.1 Monoclinic: 10.3 ± 1.1
900	Crystalline Tetragonal phase: 88.8% Monoclinic phase: 11.2%	Tetragonal: 24.1 ± 0.2 Monoclinic: 13.2 ± 1.1
1000	Crystalline Tetragonal phase: 88.9 Monoclinic phase: 11.1%	Tetragonal: 37.7 ± 0.3 Monoclinic: 13.8 ± 1.0

As expected (table 4.5), the crystallite size increases with increasing calcination temperature for both the monoclinic and tetragonal structures. With increasing calcination temperature, the powder becomes more crystalline as shown in figure 4.11 by the decrease in peak broadness. Due to grain growth at higher temperatures some t-m transformation occurs during cooling from 800°C onwards and is indicated by the formation of monoclinic peaks in figure 4.11 and quantitatively shown in table 4.5.

4.3.3. SEM of the co-precipitated 3mol% yttria stabilised ZrO_2 powder

SEM micrographs were obtained on the co-precipitated powders to determine the morphology and particle size of the powder.

Figure 4.12 below shows a micrograph of 3Y-ZrO_2 powder calcined at 900°C for 1 hour. It shows agglomerates made up of zirconia spherical particles. However the primary particles can be seen to be below 0.1μm in size (see fig. 4.12). This is consistent with the results displayed in table 4.5.

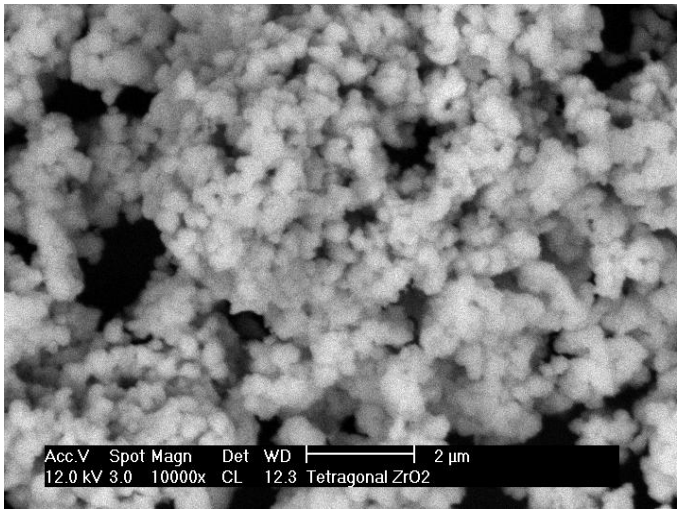


Figure 4.12: Electron micrograph of the prepared 3 mol % yttria – stabilised zirconia calcined at 900°C for one hour.

4.3.4. Particle size distribution of the co-precipitated powder

This powder was synthesized using the procedure described in section 3.1.1. The powder was then calcined at 900°C for one hour in a muffle furnace and then subjected to the same treatment as described in section 4.1.3 for the particle size analysis. Figure 4.13 shows the particle size distribution of the co-precipitated powder prior to milling.

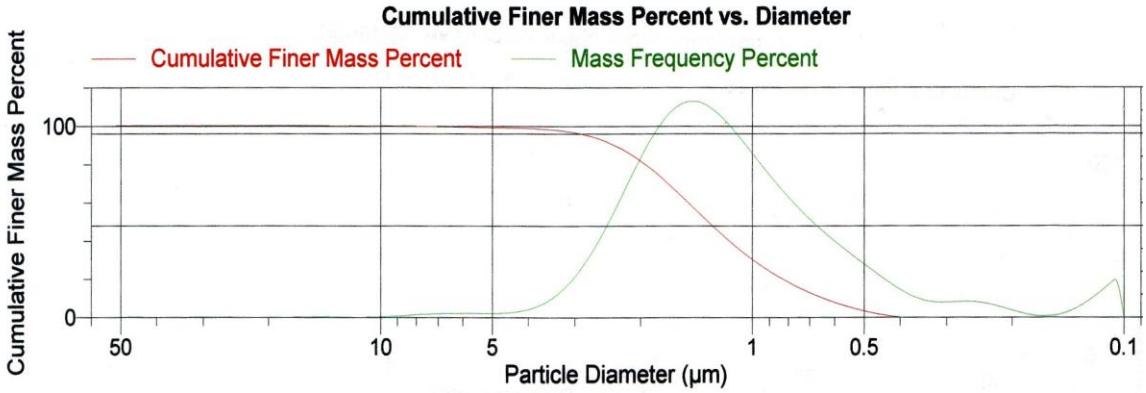


Figure 4.13: Particle size distribution of the co-precipitated powder calcined at 900°C prior to milling

The percentiles are as follows: d_{80} = 1.94µm; d_{50} = 1.31 µm; d_{10} = 0.64 µm. Figure 4.13 shows a monomodal particle size distribution showing a single peak with a maximum of

1.31 µm. This shows a fair amount of particle agglomeration compared to the primary crystallite size shown in the XRD results in table 4.5 and the line broadening shown in figure 4.11. This correlates with SEM micrograph (figure 4.12) which shows agglomerates made up of fine primary particles. As mentioned in section 4.1.3 due to the strength of the agglomerates the particle size distribution reflects the size of the agglomerates rather than the primary particles even after sonication.

After milling for approximately 8 hours at 300rpm, the particle size was reduced significantly as shown in figure 4.14:

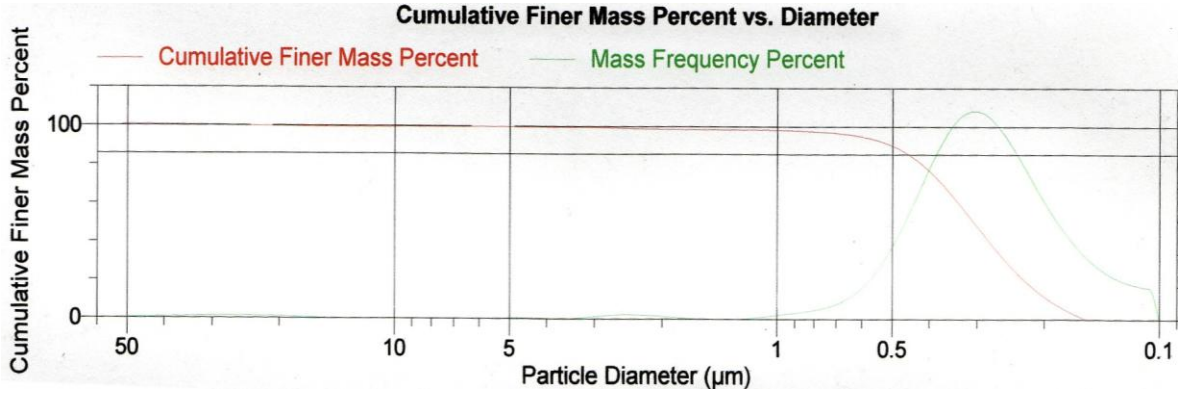


Figure 4.14: Particle size distribution of the co-precipitated powder after 8 hours of milling.

The percentiles were as follows: d_{80} = 0.41 µm; d_{50} = 0.32 µm; d_{10} = 0.19 µm. Figure 4.14 above shows a monomodal particle size distribution displaying a single peak at the maximum of 0.32µm.

Table 4.6 shows the effect of milling time on the particle size.

Table 4.6: Effect of milling time on particle size

Milling time (hours)	**Particle size d_{10}**	**Particle size d_{50} (µm)**	**Particle size d_{90}**
0	0.64 ± 0.22	1.31 ± 0.44	1.94 ± 0.70
2	0.50 ± 0.17	0.97 ± 0.32	1.58 ± 0.32
4	0.51 ± 0.44	0.71 ± 0.57	1.20 ± 0.29
6	0.29 ± 0.23	0.51 ± 0.45	0.83 ± 0.21
8	0.19 ± 0.23	0.32 ± 0.67	0.41 ± 0.20
10	0.12 ± 0.10	0.34 ± 0.12	0.39 ± 0.18

As can be seen in table 4.6, the particle size decreases as milling time increases. The particle size drops significantly in the beginning (0-2 hours) and then decreases more steadily as time progresses until it reaches a minimum of 0.3µm. After approximately 8 hours, the particle size levels off as seen with the Geratech powder and this is attributed to the strength of the particle agglomerates.

4.4. Characterization of the sintered ceramic

After compaction the green bodies were sintered at various temperatures to find the temperature that would best optimize densification and mechanical properties. The temperatures used were 1150°C, 1250°C, 1350°C, 1450°C and 1500°C for two hours. The resulting sintered ceramic is then characterized by the Archimedes technique, XRD and SEM.

XRD patterns and SEM micrographs were obtained on the sintered samples to determine the phases present, the microstructure, and the grain size.

4.4.1. Density and grain size of the ceramic after sintering

Table 4.7 shows the density of the sintered ceramic after sintering for two hours at various temperatures. The densities and open porosities were determined using the Archimedes technique and the average grain size was determined using the linear intercept method where possible.

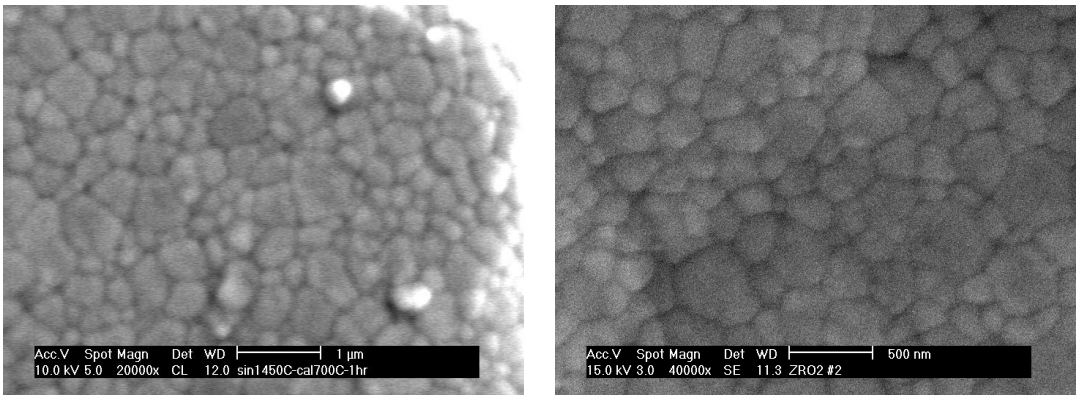
Table 4.7: Densities of the sintered ceramic as a function of temperature sintered for two hours

Sintering temperature (°C)	**Density (g/cm^3)***	**%Open porosity**	**% Density**	**AverageGrain size (µm)**
1150	**4.80**	**14.4**	**79.4**	**-**
1250	**5.41**	**8.8**	**89.6**	**-**
1350	**6.00**	**0.4**	**99.3**	**0.23 ± 0.02**
1450	**5.99**	**0.5**	**99.2**	**0.34 ± 0.02**
1500	**5.75**	**3.5**	**95.2**	**-**

* Theoretical density = 6.04g/cm^3 [29]

4.4.2. SEM Micrographs of the ceramic sintered at various temperatures

Figure 4.15 below shows the SEM micrographs of the ceramic sintered at 1350°C and 1450°C for two hours. The samples were thermally etched for 20 minutes at temperatures 50°C below the sintering temperature.



a) b)

Figure 4.15: SEM micrographs of the ceramic sintered at: a) 1450°C; b) 1350°C, for two hours

4.4.3. XRD pattern of the sintered ceramic from the co-precipitated powder

Figure 4.16 shows the XRD patterns of the ceramic sintered at 1450°C. The pattern shows a fully stabilised tetragonal phase.

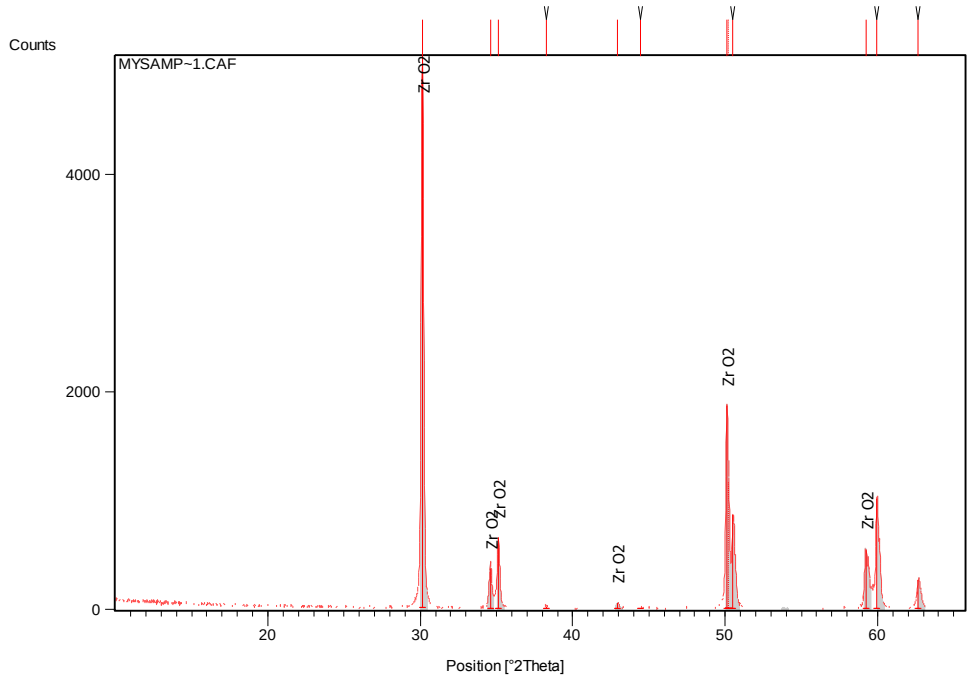


Figure 4.16: XRD pattern of the ceramic sintered at 1450°C for two hours.

SEM micrographs and XRD patterns were taken of the ceramic sintered at various temperatures to obtain the phases present and the microstructure. All the SEM micrographs regardless of sintering temperature consist of small equiaxed grains of approximately 0.1-0.5µm in diameter. The samples sintered at 1450°C and 1350°C (fig. 4.15) consist of small densely packed equiaxed grains consistent with the microstructure required for biomedical grade zirconia. Figure 4.16 shows the XRD pattern of the sample sintered at 1450°C. The sample contained the fully stabilised tetragonal structure similar to the sample sintered at 1350°C.

4.4.4. Mechanical properties of the sintered ceramic from the co-precipitated 3Y-zirconia powder

Mechanical testing such as hardness, indentation fracture toughness and density, were performed on the ceramic after being sintered at the various temperatures as described above. Table 4.8 shows a summary of the mechanical properties.

Table 4.8: Summary of the mechanical properties of the sintered ceramic at various temperatures

* There may be cubic phase present but it is very hard to distinguish between the t and c phases without vibrational spectroscopy[34]. However we still assume the original theoretical density since our target density is 6.00g/cm^3 or greater.

**theoretical density[29] = 6.04g/cm^3

Sintering temperature (°C)	Sintered density (% theoretical)**	Phases present From the XRD	Fracture toughness (MPa.m$^{0.5}$) Shetty[46]	Hardness (GPa)
1150	79.4	m, t	5.5 ± 0.1	8.2 ± 0.6
1250	89.6	t	5.7 ± 0.2	11.6 ± 0.2
1350	99.3	t	7.2 ± 0.1	13.0 ± 0.0
1450	99.2	t	7.0 ± 0.2	12.9 ± 0.1
1500	95.2	t, c*	6.5 ± 0.1	12.2 ± 0.2

The relative densities of the samples generally increase with increasing temperature but drop at 1500°C due to the possible formation of the cubic phase[34]. Hardness values increase with increasing sintering temperature and density, however the hardness for the sample sintered at 1350°C is higher than the hardness of the sample sintered at 1450°C and this can be attributed to the grain size effect as described by the Hall-Petch equation[48].

The indentation fracture toughness increases with increasing temperature until 1350°C where it drops at 1500°C. This again may be due to the presence of the cubic phase as discovered by Lange[35] which is non-transformable leading to a reduced toughness[21,22]. Other explanations include the presence of the monoclinic phase as in the sample sintered

at 1150°C as well as the relatively low densities and higher porosity achieved in these samples. The critical grain size effect also plays a vital role in the toughness of the zirconia ceramic as discussed in the literature review (section 2.4.1) and further discussed in section 5. The results in table 4.8 correspond to the results obtained from the Geratech powder in table 4.4.

4.5. Transverse Rupture Strength Results

Three-point bend tests were conducted on the ceramic made from the yttria stabilised powder supplied by Geratech as explained in section 3.2.8. Since high densities and mechanical properties were achieved with samples sintered at 1350 and 1450°C, these were the temperatures used to obtain an approximate bending strength. Due to equipment and experimental limitations only three samples were tested at each temperature. The results are reported in table 4.9.

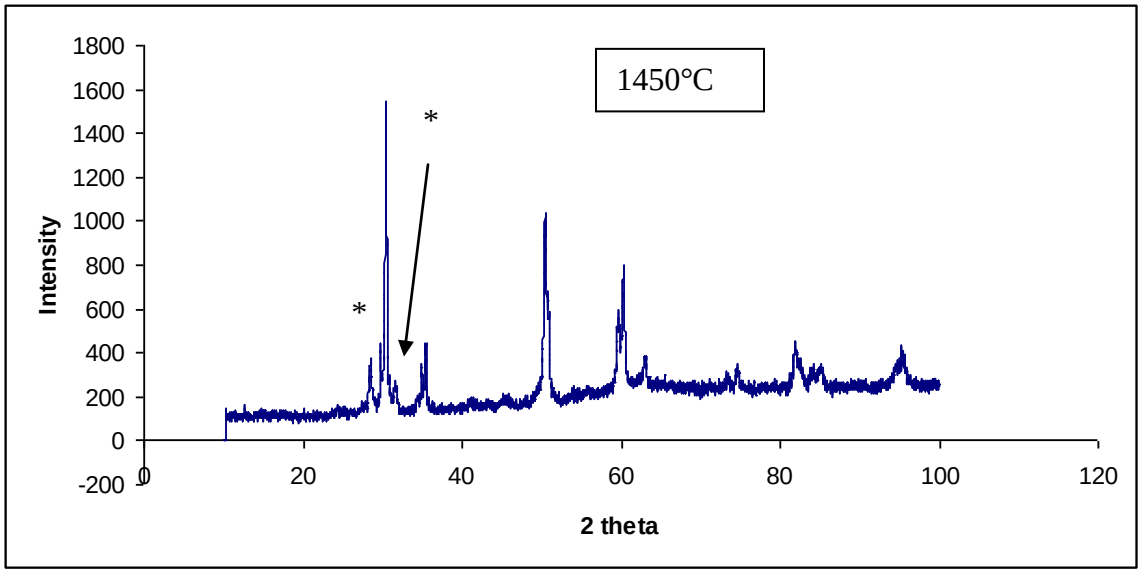
Table 4.9: TRS results of the ceramic made from the 3Y-zirconia powder from Geratech.

Sintering temperature	No.of samples	%theoretical density*	Hardness (GPa)	Toughness ($MPa.m^{0.5}$) (Shetty[46])	Bending Strength (MPa)
1450	3	99.7	12.80 ± 0.3	6.6 ± 0.19	1111 ± 23
1350	3	99.8	12.91 ± 0.6	6.3 ± 0.12	1086 ± 35

* theoretical density = 6.04 g/cm^3

Figure 4.17 shows the XRD results of the fractured surfaces of the two samples.

a)



b)

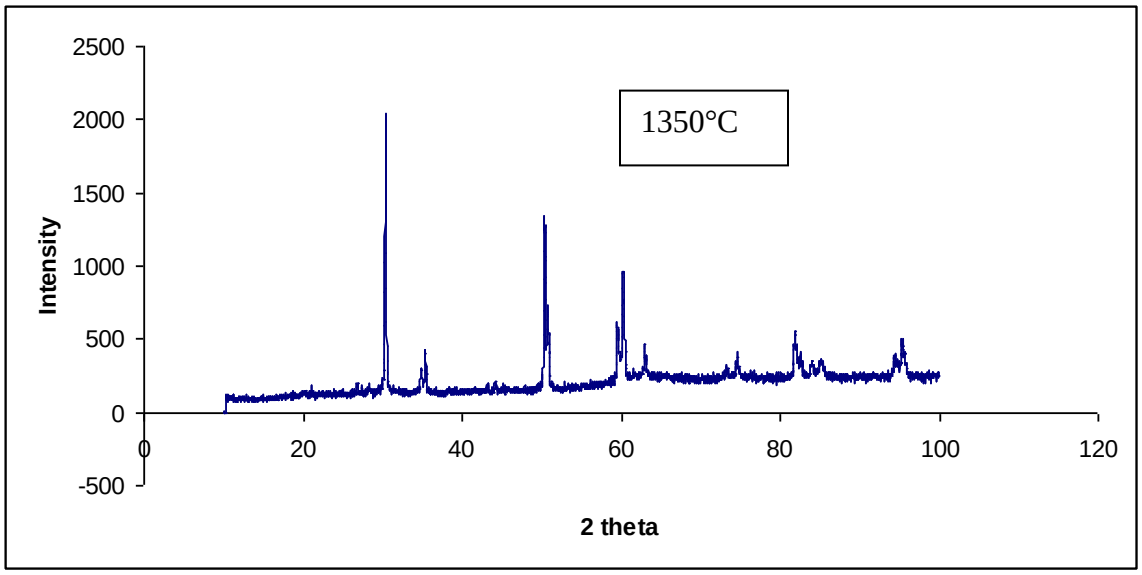


Figure 4.17: XRD patterns of the fracture surfaces sintered at: a) 1450°C and b) 1350°C. All peaks are tetragonal unless otherwise shown. *monoclinic phase

The results in table 4.9 shows that the samples sintered at 1350°C and 1450°C exhibit high strengths corresponding to the properties mentioned in section 2.4.1. The XRD results (fig. 4.17) show the transformation to the monoclinic phase on the fracture surface

for the sample sintered at 1450°C. Nettleship[34] showed that fracture strength depends on grain size and the critical grain size and subsequently the stress induced t-m transformation. This will be discussed in section 5.

4.6. The reference Zirconia biomaterial obtained from Wieland Zenotec

The green compact obtained from Wieland was sintered at various temperatures and the density was measured using the Archimedes method and is shown in table 4.10.

Table 4.10: Densities of the Wieland sintered ceramic as a function of temperature sintered for two hours

Sintering temperature (°C)	% theoretical density	Density (g/cm^3)
1450	99.5	5.97
1350	100	6.00
1250	97.2	5.83

*theoretical density according to the specification sheet = > $6.00 g/cm^3$

Figure 4.18 shows the XRD pattern of the sample sintered at 1450°C for two hours. The pattern shows a fully stabilised tetragonal phase.

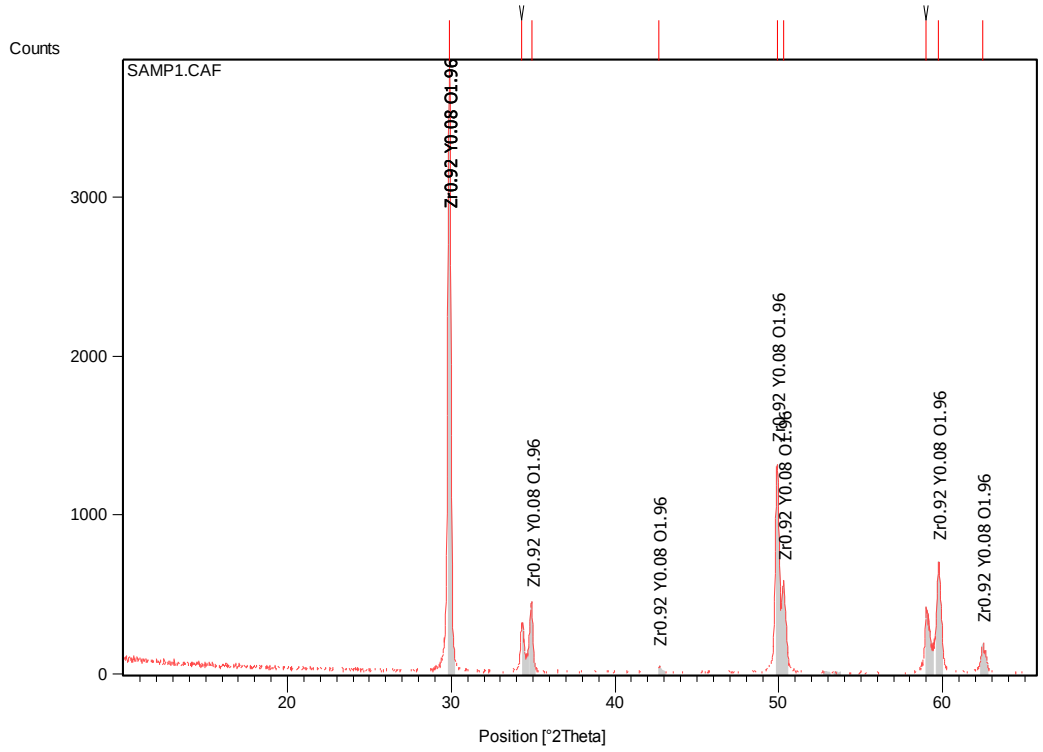


Figure 4.18: XRD pattern of the Wieland compact sintered at 1450°C for two hours.

Figure 4.19 below shows the SEM micrograph of the Wieland ceramic sintered at 1450°C for two hours. The sample was thermally etched for 20 minutes at a temperature 50°C below the sintering temperature.

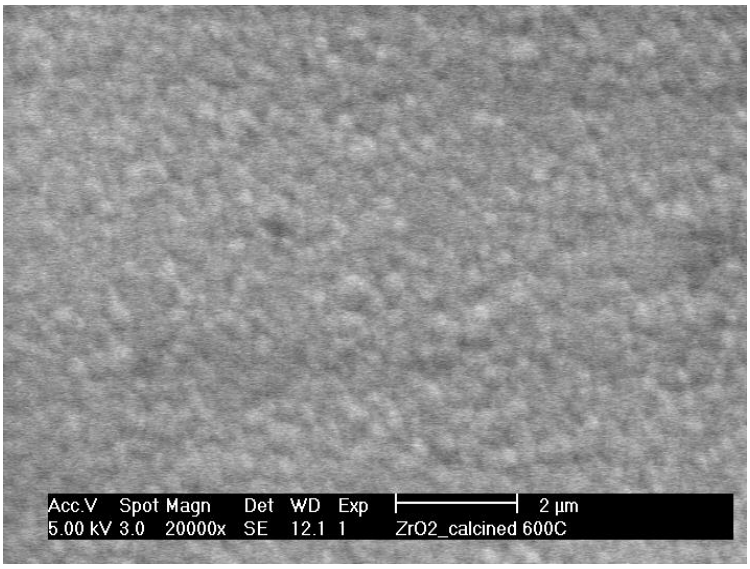


Figure 4.19: SEM micrograph of the Wieland ceramic sintered at 1450°C for two hours.

SEM micrographs and XRD patterns were taken of the Wieland ceramic sintered at 1450°C to obtain the phases present and the microstructure. The SEM micrograph (figure 4.19) consists of small densely packed equiaxed grains of approximately 0.1-0.5μm in diameter. Figure 4.18 shows the XRD pattern of this sample. As can be seen the sample contains a fully stabilised tetragonal structure.

Below in table 4.11 is a summary of the mechanical properties of the Wieland commercial disc after sintering according to the manufacturer's specifications:

Table 4.11: Summary of the mechanical properties of the Wieland Zirconia disc according to manufacturer's specifications after sintering.

Property	
Density	6.00g/cm^3
% Open porosity	0%
Hardness (GPa)	12.3 ± 0.4
Toughness (MPa.m$^{0.5}$) Shetty[46]	5.4 ± 0.1

As can be seen from the results, the mechanical properties of the ceramic made from the Geratech powders and the co-precipitated powders (tables 4.4 and 4.8 respectively) exceeds the mechanical properties of the commercial Wieland Zeno disc (3 mole% Y_2O_3 stabilised zirconia) (table 4.11).

Chapter 5: Discussion

This section gives a detailed interpretation of the results obtained in chapter 4 including the properties of the powder and the resulting ceramic.

5.1. Properties of the prepared powder

In this section results obtained from the synthesis of the yttria-stabilised solid solutions are discussed and an attempt is made to interpret the results. For all the stabilised powders synthesized, the predominant phase obtained after calcination was tetragonal with some powders containing relatively small amounts of the monoclinic phase.

5.1.1. Calcination study of the prepared powder

The X-ray diffraction patterns of the nano-powder calcined at different temperatures via the co-precipitation method are shown in figure 4.11. The significant line broadening observed in the XRD spectra of the powder indicates the formation of nano-crystals. With an increase in calcination temperature, the XRD peaks get sharper, implying an increase in crystallite size. Standard Rietveld refinement measurements[55] (table 4.5) show the crystallite sizes to be under 40 nm up to a calcination temperature of 1000°C. Figure 5.1 shows the effect of the calcination temperature on the crystallite size of the co-precipitated powder and the powders synthesized by Robert *et al.*[55]. This confirms that crystallite growth of the yttria stabilised zirconia powder is activated at the calcination temperature. The mean crystallite size of the co-precipitated powder ranges from 9 to 40 nm showing that this method is effective in the synthesis of nano-sized powders. The difference in the crystallite sizes in figure 5.1 up to a 1000°C can be attributed to the higher calcination times used by the Robert *et al.*[55], namely six hours as compared to a time of one hour for the co-precipitated powder.

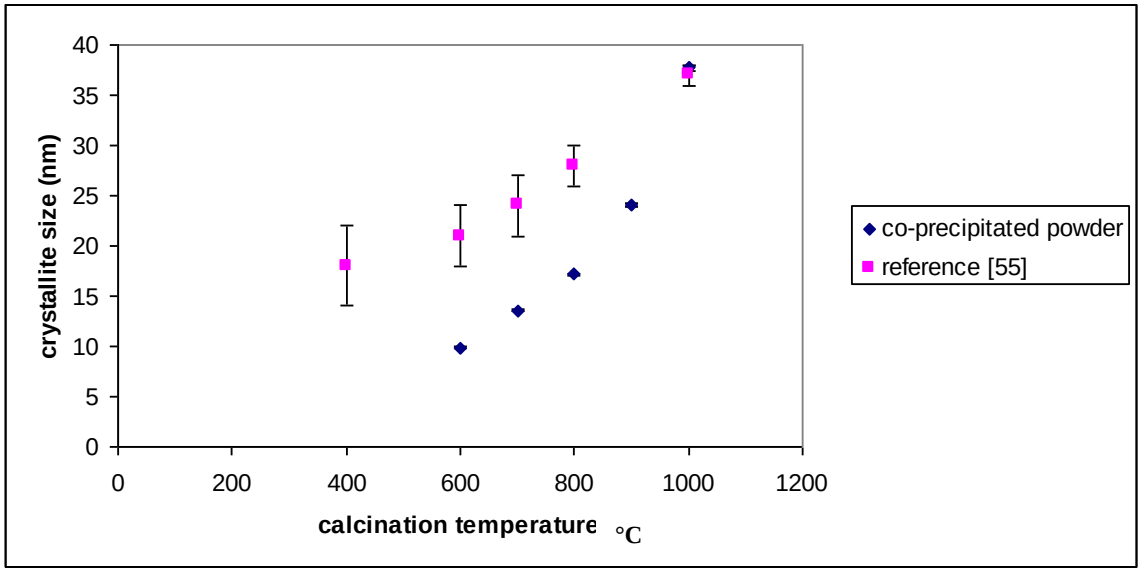


Figure 5.1: The effect of calcination temperature on crystallite size of the powder.

Bradley *et al.* (1978)[53] attributed these small crystallite sizes to the low preparation temperatures in the co-precipitation method.

A comparison of the crystallite size evaluated from the XRD and the particle size analysis (figure 4.14) shows that the particles are agglomerated. The size of the particles and the agglomerates increases with increasing calcination temperature. Scanning electron microscopy studies confirm the presence of agglomerates in the powders (Fig. 4.12) made up of very fine equiaxed primary particles in the nanometer range confirming the results of the Rietvled refinement analysis (table 4.5).

As mentioned earlier, three main stages can be seen during heating from the TGA trace (figure 4.10). The first stage corresponds to the loss of adsorbed water and solvents. The second stage corresponds to the loss of bonded water and organics and a further 5% loss mass correspond to the removal of the last $^{-}$OH group up to a 1000°C.

As seen from the DTA trace (blue trace) in figure 4.10, two main endothermic decomposition reactions can be distinguished, peaking at about 150 °C and 330°C, during which approximately 35% of the original mass is loss. It can be assumed that during this

stage, all free water and ammonia present in the sample is removed as well as the bound water and organics. A crystallization peak was expected to be seen at approximately 450-480°C[38]. However we can conclude from figure 4.11 that crystallization takes place below 600°C. Due to the slowness of the process this peak was not visible in the DTA/TGA trace in figure 4.10. These results are in agreement with previously reported data by Ramanathan *et al.* (1995)[57].

5.1.2. Compaction of the prepared powder

After calcination, powders were uniaxially cold-pressed up to 400 MPa as shown in figure 4.7. Increasing compaction pressure favors densification as shown in this figure. The density increases from 25 to 40% of theoretical density by increasing the compaction pressure from 15 - 20 MPa. However, for compaction pressures in the range 50 – 400 MPa, the green density remains stable and peaks to approximately 50%. A compaction pressure of 250 MPa which results in a green density of about 50% is used in the following study. In addition, the influence of the pressure time for this compaction pressure on the green density has been investigated and no influence was observed. These results agree well with the results found by Taha *et al.* (1995)[49] and Robert *et al.* (2003)[55] who found that a pressure of around 250 MPa to 300 MPa was sufficient to obtain a green density of approximately 50 % and to obtain subsequent high sintering densities.

5.2. Properties of the co precipitated powder and the powder supplied by Geratech

In this section results obtained from the characterization of the powder supplied by Geratech are discussed and an attempt is made to interpret the results. For the stabilised powder, the main phase was tetragonal with relatively small amounts of the monoclinic phase.

The XRD patterns of the powders are shown in figures 4.1 and 4.2. The significant line broadening that was observed in the XRD spectra and the results in table 4.1 of the powder indicates that powders consist of crystallites in the nano-meter range.

A comparison of the crystallite size evaluated from XRD and the particle size analysis (figure 4.6) shows that the particles are agglomerated. Scanning electron microscopy studies confirm the presence of agglomerates in the powders (Fig. 4.3 and 4.4) made up of very fine spherical nano-sized primary particles.

The XRD patterns of the Geratech stabilised powder (figure 4.2) and the synthesized powder (figure 4.11) both show the predominant phase to be tetragonal with some of the powders calcined at the lower temperatures containing 100% of the tetragonal phase. The XRD pattern of the Geratech powder shows two distinct monoclinic peaks whereas the synthesized powder displays a single monoclinic peak with less intensity than the Geratech powder. The Rietveld refinement results of the Geratech powder and the synthesized powder are shown in tables 4.1 and 4.5 respectively. The percentage of tetragonal phase present decreases as the calcination temperature increases ranging from 100% at 600°C down to 88% at 1000°C (figure 5.2) whereas the Geratech powder contains approximately 85% tetragonal phase.

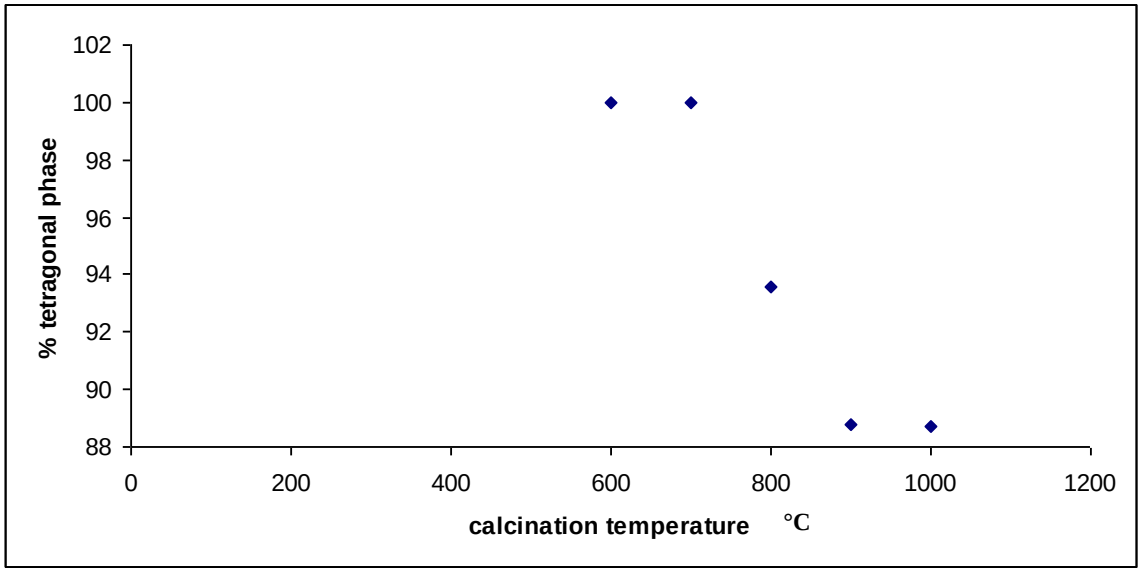


Figure 5.2: % Tetragonal phase as a function of calcination temperature for the co-precipitated powder

The difference in the phase composition between the two powders can be attributed to the different calcination temperatures used as well as the time used for calcination. As discussed in section 2.4 of the literature review, higher temperatures lead to grain growth

which leads to the formation of the monoclinic phase at the expense of the tetragonal phase.

SEM micrographs of the two powders reveal a similar morphology consisting of agglomerates made up of very fine primary spherical particles showing that a similar co-precipitation technique may have been used in the synthesis of the Geratech powder.

Measurements of the dimensions of the pressed pellet were taken for both the Geratech and the co-precipitated powder over a range of samples and the green densities ranged from 48 – 52% for all samples pressed at 250 MPa.

5.3. Properties of the sintered ceramic

The properties of the sintered yttria-stabilised zirconia ceramics have been summarized in the results section in chapter 4. It is clear from the results obtained that the properties of the ceramic depend on the resulting microstructure of the sintered material. In particular the best properties depend on the amount of retained metastable tetragonal phase, which depends on porosity, amount of stabiliser, and the grain size (as discussed in section 2.4.1). According to Robert *et al.* (2003)[55], there exists a correlation between the microstructure of the green compact and the density of the sintered ceramic. Usually complete densification in the sintered compact is obtained for high degree of homogeneity of the packing green compact. This is linked to the nature of the powders and may be achieved when powders have small crystallites size and are unagglomerated. Though, using wet-chemical routes, it is very difficult to obtain non-agglomerated sub-micron powders.

Geratech's work[56] showed that the nature of the agglomerate influences the pore size in the green body. Densification is high when a powder consisting of soft agglomerates is compacted. In the current case, since densification is high, it seems that the powders consist of relatively soft agglomerates.

5.3.1. Comparison of the sinterability of the Geratech, the synthesized powders, and the Wieland commercial compact

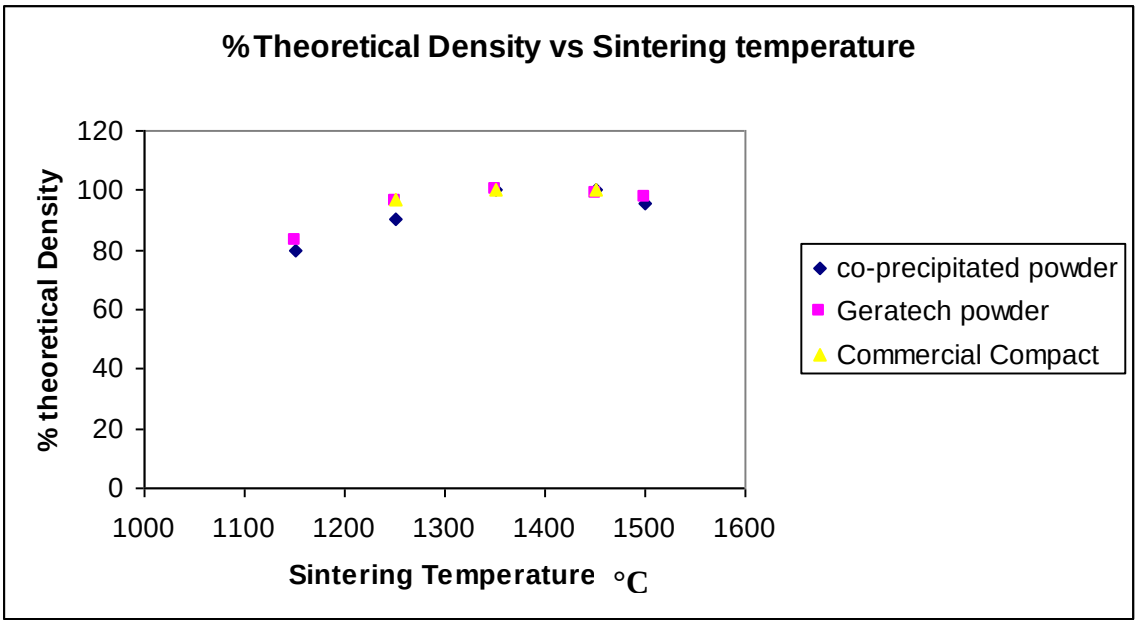


Figure 5.3: % Theoretical density as a function of sintering temperature

Figure 5.3 shows the % theoretical density as a function of temperature for the resulting ceramic from both powders and the commercial compact. The ceramic obtained from both powders show similar trends in terms of their densities. However the ceramic obtained from the Geratech powder shows slightly better densification behaviour. As mentioned, high densification depends on the homogeneity of the packing green compact. As seen in the particle size analysis of the Geratech powder and the co-precipitated powder in figures 4.6 and 4.14 respectively, the Geratech powder has a smaller particle size than the co-precipitated powder leading to better packing homogeneity and hence better densification. The commercial compact also shows high sintering densities and can also be attributed to high homogeneity packing of the green compact. Gupta *et al.* (2004)[58] and Owen *et al.* (1997)[59] have both found sintering temperatures ranging from 1350°C to 1450°C were sufficient to obtain high densities (>99%). In particular, Gupta *et al.* (2004)[58] sintered compacted powders obtained from Tosoh Co. at 1450°C for two

hours and were able to obtain a fully dense sintered ceramic. Again this is attributed to the quality of the green compact.

5.3.2. Hardness

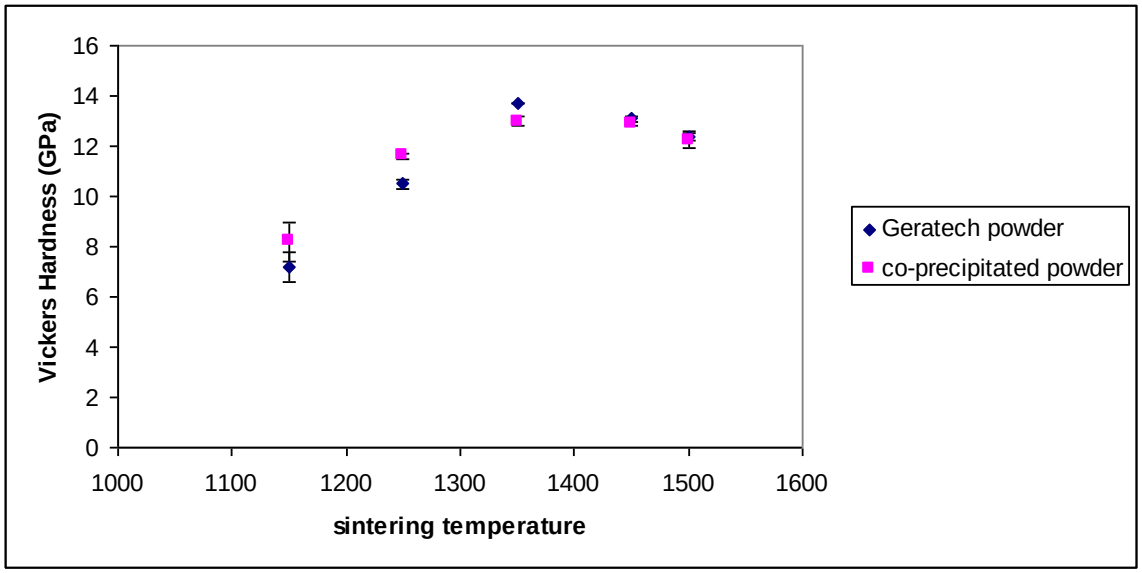


Figure 5.4: Dependence of Vickers hardness on the sintering temperature of the Geratech powders and the co-precipitated powder.

There are a number of factors influencing the hardness of a material. These include porosity, grain size, composition, and crystal structure. It is clear from figure 5.4 that as the sintering temperature increases the hardness increases and peaks at approximately 1350°C - 1450°C of sintering temperature. This trend is merely an artifact of the linear relationship between hardness and porosity[44]. Although there is grain growth as the sintering temperature increases, the hardness increase can be attributed to the reduction of porosity and monoclinic phase as temperature increases. These results agree well with results obtained from Lange (1982)[35]. The Hall-Petch equation[48] states that a smaller grain size leads to a higher hardness. This can explain the higher hardness of the samples sintered at 1350°C compared to those sintered at 1450°C. Since both have similar densities, grain size seems to be the major determining factor. The reduction of the hardness of the samples sintered at 1500°C can be attributed to grain size effects as well as the possible formation of the cubic phase as seen in section 2.2 of the literature survey.

Unfortunately, the crystal structure cannot be fully assessed since the amount of cubic phase (if any) in the sintered material is not fully known. As discussed in the literature review, it is hard to distinguish between the tetragonal and cubic phases without close examination of high angled peaks or vibrational spectroscopy[34]. Denry *et al.* (2008)[11] also stated the formation of the cubic phase is caused by the uneven distribution of the Y ions which can lead to a depletion of Y^{3+} ions at some areas enabling a t-m transformation and thus leading to a decrease in mechanical properties.

5.3.3. Fracture toughness

Several of the samples tested showed relatively high toughness as evidenced by very limited crack extension under indentation. Figure 5.5 shows the values of the fracture toughness as a function of the sintering temperature for the ceramic using the prepared powders and the Geratech powders.

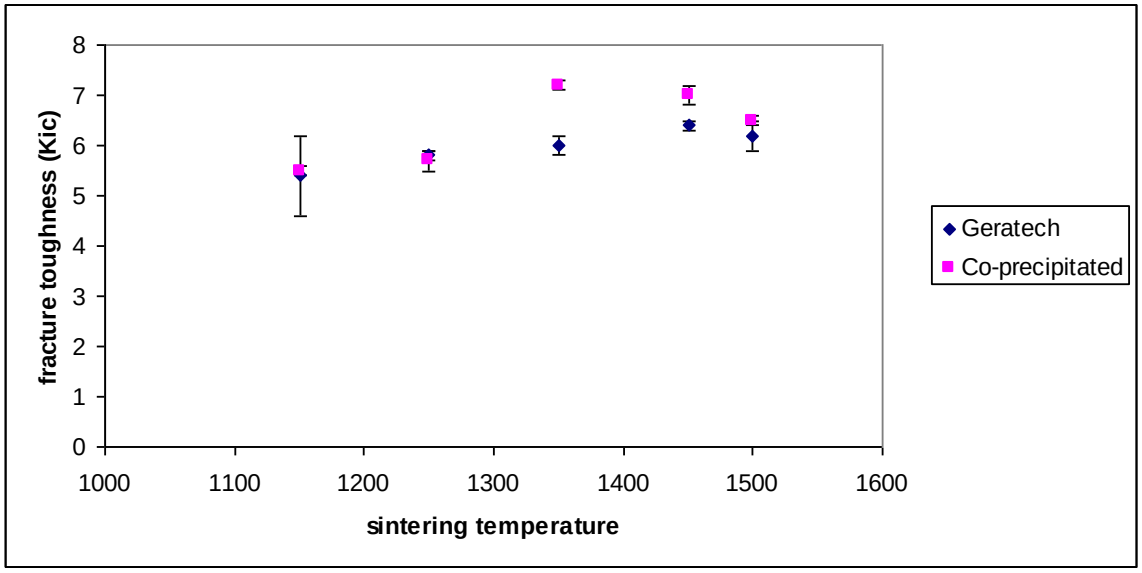


Figure 5.5: Fracture toughness as a function of sintering temperature for the ceramic using the co-precipitated and the Geratech powder.

In general, fracture toughness for the samples listed in Tables 4.4 and 4.8 increases with increasing grain size, up to a maximum value of 7.2 $MPa.m^{0.5}$ for the 3Y compositions.

Samples with larger grain sizes spontaneously undergo the tetragonal to monoclinic transformation on cooling to room temperature, and crack during fabrication. Thus, the maximum toughness (at room temperature) in fully tetragonal samples is seen at dopant/grain size combinations that correspond to the material being on the verge of spontaneous transformation (at room temperature)[44]. Thus it is evident that the samples sintered at 1350°C and 1450°C contain grains which are on the verge of transformation. The samples sintered at 1500°C may contain the cubic phase as discovered by Lange[35] which is non-transformable[21,22] thus lowering the fracture toughness (but it is difficult to distinguish between the tetragonal and cubic phase due to its identical patterns without vibrational spectroscopy[17]). The Geratech samples show lower fracture toughness values as compared to the co-precipitated samples. This is attributed to the lower average grain size of the Geratech samples (tables 4.3 and 4.7).

Away from the transformation boundary, increasing stabilization of the tetragonal phase by even smaller grains yields fracture toughnesses that approach the toughness of the undoped monoclinic material, which is also non-transformable as in the case for the samples sintered at 1250°C and 1150°C. Lower densities also contribute to the low toughness for these materials.

The reduction in toughness that occurs as a result of being far from the phase equilibrium condition is significant about a factor of five[44]. The results of Eichler *et al.*[54] on micro-grained ceramics in the 2–3 mol% Y_2O_3 doping range have some bearing on the present study. In his work, toughness is observed to reach its maximum value just prior to the phase transformation boundary. Furthermore, the location of the toughness maximum shifts systematically to larger grain sizes with greater amounts of yttria doping. In addition, Gupta *et al.* [58] sintered compacted 3Y-ZrO_2 powders obtained from Tosoh Co. at 1450°C for two hours and found, using a similar method of indentation, that fracture toughness increases with grain size up to a maximum prior to the phase transformation boundary. The results obtained in this project are similar and agree with the results reported by Gupta *et al.*[58] and Eichler *et al.*[54].

The present study shows that it is possible to achieve high toughnesses in nanocrystalline ceramics, but it requires a very precise dopant/grain size combination that places the ceramic very near the phase transformation boundary.

5.4.4. Fracture Strength

The fracture strength results for the treated specimens are shown in table 4.9. For the samples sintered at 1450°C and 1350°C the fracture strengths were 1111MPa and 1086MPa respectively. A statistical analysis (t test) using excel was performed on the data and revealed no statistical differences between the two sets using a 95% confidence interval. Firstly, for ceramic materials, an increase in strength is found for most materials with decreasing grain size[48]. Secondly, below a critical grain size, a change in the fracture criterion can be expected that may increase the strength of the material. The third contribution is the observed decrease in transformation-induced toughening with decreasing grain size. Eichler *et al.*[54] contains the influence of grain size on the three point bend test strength and found that strength increases with increasing grain size after which it decreases after passing a certain grain size. The grain size influence is related to the critical grain size for constrain of the phase transformation during mechanical loading. The decrease is caused by premature transformation, which causes microcracking and lowers the fracture strength. The sample sintered at 1350°C consists of smaller grains than the sample sintered at 1450°C, however the XRD pattern of the sample sintered at 1450°C (figure 4.20) shows the presence of the monoclinic phase on the fractured surface. This confirms that transformation toughening is a major mechanism controlling the fracture strength, dominating over all other grain size effects. These results agree with findings made by Eichler *et al.* [54]. Unfortunately, due to equipment and time limitations, only a few samples could be tested for fracture strength.

Chapter 6: Conclusions and Recommendations

6.1. Conclusion

Powders synthesized using a co-precipitation method as well as the powders supplied by Geratech consisted of nano-particles as shown by the Rietveld analysis and the SEM micrographs. The influence of the thermal treatment on the characteristics of the powder (crystallite size, phase composition) were assessed and studied. After thermal treatments, powders were characterized using SEM and XRD. Powders with crystallite sizes as small as 9nm were obtained depending on the thermal treatment. Both powders consisted of agglomerates made up of small nano-sized spherical particles. XRD results showed that the Geratech powder consisted both of the tetragonal phase (88%) and monoclinic phase (12%). The co-precipitated powder consisted of 100% tetragonal phase for powders subjected to lower calcination temperatures (600°C and 700°C). As the calcination temperature treatment increased, the tetragonal content decreased.

After calcination treatments, both the co-precipitated and Geratech powders were milled using an attritor mill to break down the agglomeration of the particles and to prepare the powder for the subsequent compaction process. The co-precipitated powder took approximately 8 hours of milling to reach an average particle size of 0.3μm and the Geratech powder took approximately 10 hours. This was attributed to a higher calcination temperature used for the Geratech powder as evidenced by the higher monoclinic content in the XRD. Commercial grade powder from Tosoh Co. generally consists of spherical granules of particle size 0.3μm with minimal or no agglomeration present compared to the relatively high amount of agglomerations present in the co-precipitated powder and the Geratech powder. This is attributed to the latest technology and hydrolysis processes used in the preparation of the Tosoh powder.

These nano-crystalline powders were then compacted to produce the green bodies. A green density ranging from 48-52% was achieved for the green compacts. It was

determined that a high density (>99%) and sub-micron equiaxed grains could be simultaneously achieved by sintering at temperatures 1350°C - 1450°C in air.

Additionally, the mechanical properties of the ceramic were the highest for the samples sintered at these temperatures. This was attributed to densification, grain size effects, and phase composition as discussed in the literature review and results (chapters 2 and 4). High densities (99-100% theoretical density) were also obtained for the commercial Zeno Zirconia discs sintered within this temperature range (1350°C - 1450°C).

The sintered ceramic prepared from both powders showed mechanical properties that matched and in some cases exceeded those of the biomedical grade zirconia (table 2; literature review). In particular, the hardness values of the prepared ceramic exceeded those of the biomedical grade target at sintering temperatures ranging from 1350°C to 1450°C. High toughness values were also achieved ranging from 6-7 $MPa.m^{1/2}$ matching those values of the biomedical grade zirconia. High fracture strength values ranging from 1000-1100 MPa, although limited tests were performed due to equipment constraints, were also achieved for the samples sintered at the above temperatures. These values are within the properties of biomedical grade zirconia.

Ceramics produced from both powders and the commercial Zeno disc resulted in similar mechanical properties being achieved. XRD patterns of the ceramic showed the predominant presence of the tetragonal phase with only samples sintered at the lower temperatures (1150°C) showing modest amounts of the monoclinic phase. SEM micrographs showed sub-micron equiaxed grains for ceramics produced from both powders similar to SEM images of bio-grade zirconia.

6.2. Recommendations

For the further evaluation of the potential of the Geratech powders for bio-applications the following is recommended:

- Agglomeration of the Geratech powder has to be minimized by optimization of the calcination and milling treatments.

- In the biomedical grade zirconia specification sheet[52], Al_2O_3 (0.5wt %) was included as a sintering aid. 0.5wt % Al_2O_3 should be added to the zirconia powder during fabrication to improve densification and reduce porosity even further during sintering.

- Sintering can be done using various other techniques (eg. High pressure sintering) to have more control over grain growth thus manipulating the microstructure to optimize mechanical properties.

- Further investigations need to be conducted regarding the TRS testing since equipment limitations limited this part of the project (in terms of quantity as well the full size of the samples that adhere to the ISO standards).

Chapter 7: References

1. Richerson, D.W. (1992). *Modern Ceramic Engineering: properties, processing and use in design.* Marcel Dekker, New York.
2. Reed, J.S. (1995). *Principles of Ceramic Processing*, 2nd. John Wiley and Sons Inc. New York.
3. Chartier, T., Gervais, T., Chermant, L., Chermant, J.L., and Coster, J. (1992). *Effect of Powder Processing on Microstructure of Zirconia during Sintering.* Journal of the European Ceramic Society. Vol. 10, pp 299-305.
4. Fukuya, M., Hirota, K., Yamaguchi, O. (1994). *Sintering and Characterization of Yttria-Stabilised Cubic Zirconia with Alumina Derived from Solid Solution.* Materials Research Bulletin. Elsevier Science Ltd. Vol. 29, No. 6, pp 619-628.
5. Viazzi, C., Deboni, A., Ferreira, J.Z., Bonino, J., Ansart, F. (2006). *Synthesis of Yttria Stabilised Zirconia by sol-gel route: Influence of experimental parameters and large scale production.* Solid State Sciences. Vol. 8, pp 1023-1028.
6. Aronne, A., Marotta, A., Pernice, P., Catauro, M. (1996). *Sol-gel Processing and Crystallization of Yttria Doped Zirconia*. Thermochimica Acta. Vol. 275, pp 75-82.
7. Guazzato, M., Albakry, M., Ringer, S.P., Swain, M.V. (2004). *Strength, fracture toughness and microstructure of a selection of all-ceramic materials. PartII. Zirconia based dental ceramics.* Dental Materials. Vol. 20, pp 449-456.
8. Kisi, E.H., and Howard, C.J. (1998). *Crystal Structure of Zirconia phases and their inter-relation.* Key Engineering Materials. Vol. 1, pp 153-154.
9. Garvie, R.C., Hannink, R.H., and Pascoe, R.T. (1975). *Ceramic Steel?*. Nature (London). Vol. 258, pp 703.
10. Scott, H.G. (1975). *Phase Diagram in the Zirconia-Ytrria System.* J. Am. Ceram. Soc. Vol. 50, p 1527.
11. Denry, I., Kelly, J.R.(2008) *State of the art of zirconia for dental applications.* Dental Materials. Vol. 24, pp 299-307.
12. Hannink, R.H.J., Kelly, P.M., and Muddle, B.C. (2000). *Transformation Toughening in Zirconia containing ceramics.* J. Am. Ceram Soc. Vol. 83, pp461.

13. Sato, T. and Shimada, M. (1984). *Crystalline phase change in Yttria-Patrially Satbilised Zirconia by Low Temperature Annealing.* J. Am. Ceram. Soc. Vol 65, p 212.
14. Smith, D.K., and Nemkirk, H.W., (1965). *The crystal structure of baddeleyite (monoclinic zirconia) and its relation to the polymorphism of zirconia.* Acta Cryst. Vol. 18, p 983.
15. Moeller, T. (1956). *Inorganic chemistry.* Wiley, New York.
16. Bansal, G.K., and Heuer, A.H. (1972). *On a martensitic phase transformation in zirconia-I. Metallographic Evidence.* Acta Metall. Vol. 20, p 1281.
17. Srinivasan, R., Simpson, S.F., Harris, M.B., and Davis, B.H. (1991). *Discrepancies in the crystal structures assigned to precipitated zirconia.* J. Mater. Sci. Lett. Vol. 10, p 352.
18. Hann, R.E., Suitch, P.R., and Pentecost, J.L. (1985). *Monoclinic crystal structure of ZrO_2 and HfO_2 refined from X-ray powder diffraction data.* J. Am. Ceram. Soc. Vol 68, p 285.
19. Scott, M.G. (1975). *Phase diagram in the Zirconia-Yttria System.* J. Am. Ceram. Soc. Vol. 50, p 1527.
20. Stubican, V.S. (1988). *Advances of Zirconia.* Science and Technology of Zirconia III. Vol. 24. Edited by S. Somiya, N. Yamamoto, and H. Hanagida (The American Ceramics Society, Westerville, OH) 71.
21. Jayaratna, M., Yoshimura, M., and Somiya, S. (1984). *Subsolidus Phase relations in the Pseudoternary system ZrO_2-$YO_{1.5}$-$CrO_{1.5}$ in air.* J. Am. Ceram. Soc. Vol 67, p 240.
22. Yoshimura, M. (1988). *Phase Stability of Zirconia.* Am. Ceram. Soc Bull. Vol 67, p 1950.
23. Patil, R.N., and Sabbarao, E.C. (1970). *Monoclinic-Tetragonal phase transformation in zirconia: mechanism, pretransformation, and coexistence.* Acta. Cryst. Vol A26, p 535.
24. Heuer, A.H., Ruhle, M. (1985). *On the nucleation of the transformation in zirconia.* Acta. Metall. Vol 33, p 2101.

25. Chen, I.W., Chaio, Y.H., (1985). *Theory and experiment of martensitic nucleation in ZrO_2 containing ceramics and ferrous alloys.* Acta. Metall. Vol 33, p1827.
26. Denry, I., Kelly, J.R. (2008). *Stabilised zirconia as a structural ceramic: An overview.* Dental Materials. Vol 24, pp 289-298.
27. Ehrenfest, P. (1954). Proc. Amsterdam Academy. Vol 36, p153.
28. Becher PF, Swain MV. (1992). *Grain-size-dependent transformation behavior in polycrystalline tetragonal zirconia*. J. Am. Ceram. Soc.Vol. 75(3), pp 493–502.
29. Wakai, F., Sakaguchi, S., Matsuno, Y. (1986). *Superplasticity of Yttria stabilised Zirconia polycrystals.* Advanced Ceramic Materials. Vol. 1. No. 3, pp 259-263.
30. Gupta, T.K., Bechtold, J.H., Kuznichi, R.C., Cadoff, L.H., and Rossing, B. R., (1977). *Stabilization of tetragonal phase in polycrystalline zirconia.* J. Mat. Sci. Vol. 12, pp 2421-26.
31. Robert, C.L., Ansart, F., Deloget, C., Gaudon, M., Rousset, A. (2003). *Dense Yttria stabilised zirconia: sintering and microstructure.* Ceramics International. Vol. 29, pp 151-158.
32. Mazaheri, M., Simchi, A., Dourandish, M., Fard, F.G. (2009). *Mastering Sintering curves of a nano scale 3Y-TZP powder compacts.* Ceramics International. Vol. 35, pp 547-554.
33. Basu, B., Vleugels, J., Van Der Biest, O. (2004). *Toughness tailoring of yttria Doped zirconia ceramics.* Materials Science and Engineering. A 380, pp215-221.
34. Nettleship, I., Stevens, R. (1987). *Tetragonal Zirconia Polycrystal: An Overview.* Int. J. High Technology Ceramics. Vol. 3, pp1-32.
35. Lange, F. F., *Transformation toughening--Part 3: Experimental observations in the ZrO_2-Y_2O_3 system*. J. *Mat. Sci.*, 17 (1982), p 240.
36. Theunissen, G.S.A.M., Winnubst, A.J.A., and Burggraaf, A.J. (1992). *Effect of Dopants on the Sintering Behaviour and Stability of Tetragonal Zirconia Ceramics.* Journal of European Ceramic Society. Vol. 9, pp 251-263.
37. Hwang, S.L., Chen, I.W. (1990) J. Am. Ceram. Soc. 73. p 3269.
38. Chaim, R., Basat, G., Demyanets, A.K. (1997). *Effect of oxide additives on Grain growth during sintering of nanocrystalline zirconia alloys.* Materials Letters 35, pp 245-250.

39. Alleman, J.A., Michel, B. (1995). *Grain growth of differently doped Zirconia.* Journal of the European Chemical Society 15, pp 951-958.
40. Hwang, S. & Chen, I. (1990). *Grain size control of tetragonal zirconia polycrystals using the space charge concept,* J. Am Ceram. Sot., 73(11) pp 3269-77.
41. Chokshi, A.H. (2003). *Diffusion, diffusion creep and grain growth Characteristics of nanocrystalline and fine-grained monoclinic, tetragonal and cubic zirconia.* Scripta Materialia 48, pp 791-796.
42. Chevalier, J. (2006). *What future for zirconia as a biomaterial.* Biomaterials (27) pp 535-543.
43. Chevalier, J., Gremillard, L. (2009). *Ceramics for medical applications: A Picture for the next 20 years.* Journal of the European Ceramic Society. 29. pp 1245-1255.
44. Leon, A.B., Morikawa, Y., Kawahara, M., Mayo, M.J. (2002). *Fracture Toughness of nanocrystalline tetragonal zirconia with low yttria content.* Acta Materialia (50), pp 4555-4562.
45. Hirvonen, A., Nowak, R., Yamamoto, Y., Sekino, T., Niihara, K. (2006). *Fabrication, structure, thermal and mechanical properties of zirconia-based Ceramic nano-composites.* Journal of the European Ceramic Society 26, pp 1497 -1505.
46. Shetty, D.K., Wright, R.G., Mincer, P.N., and Claucer, P.N. (1985). *Indentation Fracture of WC-Co cermets.* J. Mater. Sci. Vol. 20, p 1875.
47. Oilo, M., Gjerdet, N.R., Tvinerreim (2008). *The firng procedure influences Properties of a zirconia core ceramic.* Dental Materials 24, p 471-475.
48. E.O.Hall. (1951). Proc. Phys. Soc., Ser. B, Vol. 64, pp. 747-753.
49. Taha, M., Palleto, J., Jorand, Y., Fantozzi,G. (1995) *Compaction and Sintering Behaviour of zirconia powders*. Journal of the European Ceramic Society 15 pp 759-768
50. International Standard ISO 14704:2000, Technical Corrigendum 1 (2004).
51. http://www.accuratus.com/zirc.html (retrieved 25 February 2010).
52. http://www.wieland-international.com/produkte/zen (retrieved 25 February

2010).

53. Bradley, D.C., Mehrotra, R.C., Gaur, D.P. (1978). *Metal Alkoxides*, Academic Press, New York.
54. Eichler, J., Rodel, J., Eisele, U., Hoffmann, M. (2007). *Effect of Grain Size on Mechanical Properties of submicrometer 3Y-TZP: Fracture strength and Hydrothermal Degradation.* J. Am. Ceram. Soc. Vol. 90. pp 2830-2836.
55. Robert, C.L., Ansart, F., Deloget, C., Gaudon, M., Roussett, A. (2003). *Dense Yttria stabilised zirconia: sintering and microstucture.* Ceramics International Vol. 29. pp 151-158.
56. www.geratech.co.za (retrieved 7 April 2010).
57. Ramanathan, S., Muraleedharan, R.V., Roy, S.K., Naya, P.K. (1995). *Dehydration and crystallization kinetics of zirconia-yttria gels.* J. Am. Ceram. Soc. Vol. 78, p 429.
58. Gupta, N., Mallik, P., Basu, B. (2004). *Y-TZP ceramics with optimized Toughness: new results.* Journal of alloys and compounds. Vol. 379, pp 228-232.
59. Owen, D.M., Chokshi, A.H. (1997). *Final stage free sintering and sinter forging behaviour of yttria stabilised tetragonal zirconia.* Acta. Mater. Vol. 46. pp 719-729.

Chapter 8: Appendices

Appendix 1: Calculation of mass of yttrium chloride to be added to the zirconium oxychloride solution:

Mass of zirconium oxychloride (ZOC) crystals used: x

Percentage ZrO_2 in ZOC crystals: 35%

Mass of ZrO_2 = x * 0.35

Moles of ZrO_2 = 0.35x * (molar mass ZrO_2)

% Moles Y_2O_3 required = 3 %

Moles Y_2O_3 required = [3/(100-3)] * mole ZrO_2

Mass Y_2O_3 required = [Moles Y_2O_3 * Molar mass Y_2O_3(225.81)]/1000

Mass Yttrium Chloride required =

[2 * molar mass of YCl_3/molar mass of Y_2O_3] * mass of Y_2O_3 required

Appendix 2: EDS analysis of ZrO_2

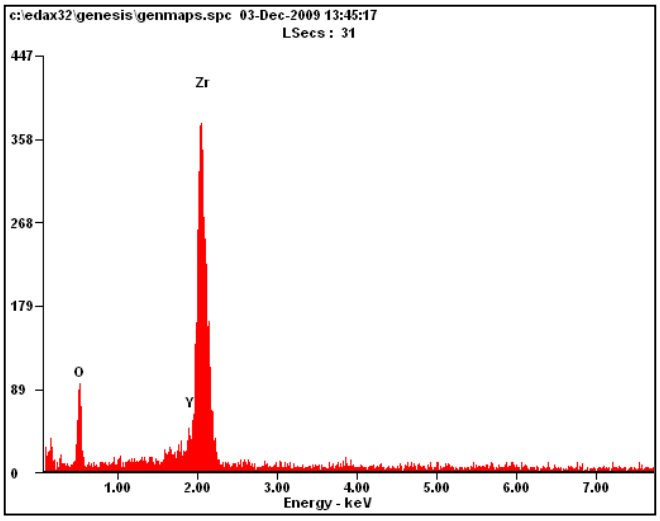


Figure A1: EDS analysis of the co-precipitated powder

EDS was performed on the powder shown in the results section. All powders showed a similar EDS pattern. High voltage was used to try and detect the presence of yttrium but due to low quantities yttrium used, it could barely be detected.

Appendix 3: Properties of the Wieland Zeno Zirconia Disc[52]

These discs are produced and manufactured in Germany by Wieland International and are supplied as partially sintered discs with varying degrees of thicknesses. The supplied discs are approximately 50% of theoretical density (6.04g/cm^3). According to the manufacturer's specification sheet their composition consists of:

ZrO_2	95 wt%
Al_2O_3	1 wt%
Y_2O_3	4 wt%